A Linear Theory for Jet Streak Formation Due to Zonal Momentum Forcing in a Stably Stratified Atmosphere

RONALD P. WEGLARZ AND YUH-LANG LIN

Department of Marine, Earth, and Atmospheric Sciences, North Carolina State University at Raleigh, Raleigh, North Carolina

ABSTRACT

A perturbation potential vorticity (PV) theory is developed to investigate the three-dimensional, time-dependent, linear geostrophic adjustment of a stably stratified, Boussinesq atmosphere that is disturbed from (i) quiescent equilibrium due to a localized, unbalanced, zonal wind anomaly and (ii) geostrophic equilibrium of the uniform zonal flow due to an isolated couplet of acceleration–deceleration forcing. This prescribed zonal momentum forcing propagates downstream at a speed c that is less than the basic-state zonal flow speed U and physically represents the parameterized effects of nonlinear inertial advection.

Transient, dispersive inertia–gravity waves in all fields are essentially removed during the early stage of the response associated with the initial value problem. The steady-state equilibrium that conserves the initial perturbation PV is a localized, geostrophic zonal jet with meridionally confluent (diffluent) flow in its entrance (exit) region. This jet is supported by a couplet of perturbation low and high pressure north and south of the zonal jet core, respectively. There exist no steady-state ageostrophic winds and vertical motions once balanced equilibrium is reached. This long-term asymptotic response characterizes a localized *linear thermal wind balance* among the baroclinic perturbations that will not be preserved in the nonlinear initial value problem.

The forced response for a uniform, stably stratified, zonal flow whose Rossby number is $Ro_U = (U - c)/2af = 0.1$, where a is the half-width of the prescribed zonal momentum forcing as seen by a Galilean observer traveling at the speed $c < U$, shows many similar characteristics with the forced shallow water flow response of Weglarz. In particular, the early response for $t \leq \tau = 2a/(U - c)$ is characterized by a pair of easterly and westerly zonal jet streaks produced by flow acceleration/deceleration in the forcing entrance/exit region. The mass field quickly adjusts to the sub-Rossby scale ($a \ll 2d_{jet}N/f$) perturbations in the wind field, forming a pair of high–low couplets that geostrophically support the isolated zonal jets. For $t > \tau$, the easterly zonal jet is advected downstream at the relative velocity $U - c$, leaving an isolated, meso-α-scale, westerly zonal jet streak in the vicinity of the forcing center. The ageostrophic winds characterize a mesoscale cyclonic circulation that circumvents the forcing center. The divergence associated with this circulation produces a four-cell pattern of vertical motion that flanks the core of the zonal jet streak. This pattern of steady, *externally forced,* vertical motion is *reversed* from the pattern normally inferred from traditional nonlinear quasigeostrophic jet streak dynamics because the accelerations produced by the imposed zonal momentum forcing dominate those produced by local time rate of change and linear inertial advection of the geostrophic flow.

1. Introduction

If an upper-level midlatitude jet streak exists in a developing synoptic-scale baroclinic wave and propagates downstream toward a quasi-stationary ridge in the geopotential height field, the flow becomes highly ageostrophic (Kaplan and Paine 1977). Because the divergence tendency of this flow cannot be neglected, inertia–gravity waves are excited as the atmosphere attempts to reestablish a quasigeostrophic balance. The ageostrophic winds have the effect of transferring mass from the anticyclonic to the cyclonic side of the jet streak exit region. This thermally direct circulation converts available potential energy into zonal kinetic energy, causing the flow to accelerate alongstream rather than to decelerate as it would in regions where curvature effects are less pronounced. Such strong upper-level geostrophic adjustment mechanisms are a common characteristic of synoptic-scale environments where severe weather forms, and are currently believed to be responsible for the generation of observed meso-α/β-scale inertia–gravity waves (e.g. Uccellini and Koch 1987).

The geostrophic adjustment problem resulting from nonlinear inertial advective forcing (e.g., Van Tuyl and Young 1982), orographic forcing (e.g., Kaplan et al. 1994a, 1995), or thermal forcing associated with low- to midlevel latent heat release from nearby mesoscale convective systems (e.g., Kaplan et al. 1994b) is an initial-value problem. The resulting evolution towards a new balance can be considered as a *restructuring* of the preexisting meso-α- to synoptic-scale jet streak. Re-

Corresponding author address: Dr. Ronald P. Weglarz, Dept. of Marine, Earth, and Atmospheric Sciences, Campus Box 8208, North Carolina State University at Raleigh, Raleigh, NC 27695-8208.
E-mail: Ronald_Weglarz@ncsu.edu

cent numerical simulations by Kaplan et al. (1994a,b; 1995) indicate that the subsynoptic jet streak geostrophic adjustment process is not well resolved by conventional upper-level rawinsonde data. Yet it tends to play a major dynamical role in preconditioning the mesoscale environment for the formation of severe weather.

The classic conceptual models of midlatitude synoptic-scale jet streaks and their associated ageostrophic circulations (University of Chicago Dept. of Meteorology 1947; Namias and Clapp 1949; Riehl et al. 1952; Murray and Daniels 1953; Reiter 1969) are based on either semi- or quasigeostrophic dynamics that neglect the divergence tendencies necessary for the excitation of inertia-gravity waves. In reality, an unperturbed jet streak is in quasi-balance with the divergence associated with the zonal wind gradient and the ageostrophic entrance and exit region circulations responsible for its downstream propagation (e.g., Van Tuyl and Young 1982; Bluestein 1993).

Most geostrophic adjustment studies have focused on the adjustment of an initially unbalanced, temporally impulsive, small amplitude, ageostrophic perturbation introduced into a motionless basic state (see Blumen 1972; Gill 1982 and references therein). However, midlatitude jet streaks are often never observed in motionless or quiescent basic-state flows. Therefore, advective effects should be taken into account, especially if jet streak adjustments or the dynamics of jet streak formation are formally considered. Some work has been done to include the effects of basic-state zonal flows. Schubert et al. (1980) used the two-layer model developed by Paegle (1978) to investigate the response of a flow in gradient wind balance to axisymmetric mass and momentum perturbations with application to the dynamics of tropical cyclones. Duffy (1990) has investigated the effects of vertical wind shear on one-dimensional mass and momentum perturbations in an idealized, two-layer rigid-lid model (Williams 1965). Vallis (1992) recently has shown for a shallow water flow that a state of nondivergent geostrophic equilibrium constitutes the minimum energy state allowable under the constraint of potential vorticity conservation.

Nevertheless, it is important to understand theoretically both the free and forced transient responses as well as the subsequent adjustment to balanced equilibrium that rotating homogeneous and continuously stratified flows undergo due to the impulsive and temporally continuous addition of localized zonal momentum. In this paper, unbalanced zonal wind anomalies and independently propagating zonal momentum forcings are introduced into a quiescent, stratified fluid and a uniform, geostrophically balanced, zonal flow, respectively, to understand the role of adiabatic geostrophic adjustment processes in the formation of midlatitude meso-α- to synoptic-scale jet streaks. This line of inquiry is pursued primarily in order to bridge the gap between the results of classic adjustment theory

(e.g., Rossby 1938; Cahn 1945), which deals with idealized ageostrophic initial states evolving in motionless atmospheres whose mass and momentum fields generally are not very representative of midlatitude jet streaks, and the role played by tropospheric jet streaks as upper-level forcing mechanisms in the nonlinear evolution of complex baroclinic environments (e.g., Uccellini and Johnson 1979; Uccellini and Koch 1987; Zack and Kaplan 1987; Koch and Dorian 1988; Kaplan et al. 1994a,b;1995).

The physical mechanisms responsible for the initial stages of midlatitude jet streak genesis can be understood by theoretically investigating the geostrophic adjustment of an unbalanced, small-amplitude zonal wind anomaly introduced impulsively into a continuously stratified fluid or by imposing a prescribed zonal momentum forcing that is chosen to represent fundamentally *nonlinear processes* in the interior of the stratified flow. The purpose of studying the former linear initial-value problem is to (a) generalize the linear homogeneous shallow water theory of Barwell and Bromley (1988) to a continuously stratified fluid, (b) generalize the two-dimensional linear stratified theory of Bolin (1953) by considering a three-dimensional impulsive momentum source, and (c) complement the recent linear theory of Luo and Fritts (1993) by studying the three-dimensional *structure* of the adjustments and the evolution of both the geostrophic and ageostrophic wind perturbations as balanced equilibrium is approached.

The second approach reduces the nonlinear initial-value problem to a linear forced problem by transferring the nonlinear inertial advective terms to the right side of the zonal and meridional momentum equations, similar to the approach adopted in linear theories developed to *parameterize* the effects of nonlinearity during the geostrophic adjustment of rotating, homogeneous, shallow-water models (see Blumen 1972 for a detailed review). Because it is well known that the transverse ageostrophic entrance and exit region circulations at the jet core level are due to inertial advective processes (e.g., Uccellini and Johnson 1979; Bluestein 1993), investigation of the forced linear geostrophic adjustment of a rotating, stratified flow where the effects of nonlinear inertial advection are parameterized in terms of momentum forcing may help in understanding the dynamics of midlatitude jet streak formation. Linear perturbation theory, which has been so successful in understanding the dynamics of orographically (e.g., Smith 1979, 1989) and thermally (e.g., Lin 1994a,b) forced gravity waves, is used to derive the appropriate set of *coupled* wave equations within the context of potential vorticity theory. The theory is then applied to both the initial value and forced geostrophic adjustment problems associated with impulsive and temporally continuous zonal momentum forcings in a stably stratified Boussinesq atmosphere.

Specifically, we investigate the three-dimensional linear response of a uniform, vertically unbounded (infinitely deep), continuously stratified, Boussinesq flow to momentum forcing. This work is a natural extension of, and complementary to, the recent problem of meso-α-, β-, and synoptic-scale jet streak formation due to prescribed zonal momentum forcing in a uniform, geostrophically balanced, shallow water flow addressed by Weglarz (1994). Section 2 outlines the general theory, after which the linear initial value problem is formulated and the response of a quiescent, stably stratified fluid to an impulsively introduced ageostrophic zonal wind anomaly is discussed. Section 3 introduces the linear theory developed to investigate the geostrophic adjustment of a uniform, geostrophically balanced, zonal flow to a uniformly propagating *dipole* of zonal momentum forcing traveling at the speed c ($<U$). The structure of the dipole forcing is specifically chosen to parameterize the effects of nonlinear inertial advective processes and produces localized regions of acceleration (deceleration) upstream (downstream) of the forcing center. The response should therefore represent the interaction that occurs in the real atmosphere as an isolated midlatitude jet streak forms in the background synoptic-scale flow. Section 4 summarizes the major findings.

2. Potential vorticity theory and the initial-value problem

a. The linearized wave equations

The linearized equations expressing the conservation of zonal, meridional, and vertical momentum, mass, and thermodynamic energy governing the response of hydrostatic, baroclinic perturbations in a uniform, continuously stratified, Boussinesq flow on an f-plane in the presence of external momentum and thermal forcing are

$$\frac{Du'}{Dt} - fv' + \frac{1}{\rho_0}\frac{\partial p'}{\partial x} = F_x, \tag{1}$$

$$\frac{Dv'}{Dt} + fu' + \frac{1}{\rho_0}\frac{\partial p'}{\partial y} = F_y, \tag{2}$$

$$\frac{1}{\rho_0}\frac{\partial p'}{\partial z} - \frac{g}{\theta_0}\theta' = 0, \tag{3}$$

$$\frac{\partial u'}{\partial x} + \frac{\partial v'}{\partial y} + \frac{\partial w'}{\partial z} = 0, \tag{4}$$

$$\frac{D\theta'}{Dt} + \frac{N^2\theta_0}{g}w' = \frac{\theta_0}{c_p T_0}Q, \tag{5}$$

where $D/Dt = \partial/\partial t + U\partial/\partial x + V\partial/\partial y$; F_x and F_y (m s^{-2}) are zonal and meridional momentum forcings, respectively, which are taken here to represent the a priori assumed known parameterized effects of nonlinear inertial advection ($F_x = -\mathbf{V}'\cdot\nabla u'$, $F_y = -\mathbf{V}'\cdot\nabla v'$, where

$\mathbf{V}' = u'\mathbf{i} + v'\mathbf{j} + w'\mathbf{k}$) in the interior of the stratified flow, and Q is the diabatic forcing [J kg^{-1} s^{-1}]. Other symbols have their conventional meanings.

The presence of a nonzero basic-state flow incorporates the physical mechanisms of perturbation geostrophic vorticity advection $-\mathbf{U}\cdot\nabla\zeta_g'$ and horizontal temperature advection $-\mathbf{U}\cdot\nabla\theta'$. This is important in more realistic problems than addressed here. They include (i) a preexisting potential vorticity (PV) anomaly that can interact with an isolated PV *dipole* through advection by the basic-state flow, (ii) the presence of external forcings in addition to an initial perturbation PV distribution, and (iii) self-advection due to nonlinear processes. These physical mechanisms play an essential role in the development of midlatitude synoptic-scale systems when the zonal wind anomaly is viewed as an upper-level forcing interacting with low-level diabatically and orographically forced PV anomalies (e.g., Hoskins et al. 1985).

The potential vorticity equation may be derived from (1)–(5):

$$\frac{Dq'}{Dt} = F_\zeta + \frac{fg}{N^2 c_p T_0}\frac{\partial Q}{\partial z}. \tag{6}$$

In (6), the perturbation potential vorticity is

$$q' = \zeta' + \frac{f}{\rho_0 N^2}\frac{\partial^2 p'}{\partial z^2}, \tag{7}$$

which, in general, has contributions from both the induced relative vorticity and the perturbation stratification [$\partial\theta'/\partial z$, see (3)]. Although the perturbation PV (7) has a form similar to that of quasigeostrophic theory (e.g., Gill 1982), the relative vorticity perturbation ζ' implicitly includes geostrophic *and* ageostrophic components (i.e., $\zeta' = \zeta_g' + \zeta_{ag}'$). Here, $F_\zeta = \partial F_y/\partial x - \partial F_x/\partial y$ is the time rate of vorticity generation associated with the external momentum forcing and is similar to that adopted by Zhu and Holton (1987). In the absence of external forcing, the perturbation PV is conserved following the motion of the basic-state flow. The linearized wave equations governing the baroclinic perturbations $\mathbf{u}' = (u', v', w')$, p', and θ' may be written collectively as

$$L\phi'(\mathbf{r}, t) = S(\mathbf{r}, t), \tag{8}$$

where $\mathbf{r} = (x, y, z)$; $\phi' = \mathbf{u}'$, p', or θ'; L is a differential operator,

$$L = \left\{\left[\left(\frac{\partial}{\partial t} + U\frac{\partial}{\partial x} + V\frac{\partial}{\partial y}\right)^2 + f^2\right]\frac{\partial^2}{\partial z^2} \right.$$
$$\left. + N^2\left(\frac{\partial^2}{\partial x^2} + \frac{\partial^2}{\partial y^2}\right)\right\}, \quad \text{if } \phi' = (\mathbf{u}', p', \text{ or } \theta'); \tag{9}$$

and $S(\mathbf{r}, t)$ is a source term that describes the evolution of the initial perturbation PV distribution and forcings associated with momentum and diabatic sources,

$$
S(\mathbf{r}, t) = \begin{cases}
-N^2\dfrac{\partial q'}{\partial y} + \dfrac{\partial^2}{\partial z^2}\left(\dfrac{DF_x}{Dt} + fF_y\right) - \dfrac{g}{c_p T_0}\dfrac{\partial^2 Q}{\partial z \partial x}, & \text{if } \phi' = u' \\[3mm]
N^2\dfrac{\partial q'}{\partial x} + \dfrac{\partial^2}{\partial z^2}\left(\dfrac{DF_y}{Dt} - fF_x\right) - \dfrac{g}{c_p T_0}\dfrac{\partial^2 Q}{\partial z \partial y}, & \text{if } \phi' = v' \\[3mm]
-\dfrac{\partial}{\partial z}\left(\dfrac{DF_\delta}{Dt} + fF_\zeta\right) + \dfrac{g}{c_p T_0}\nabla_H^2 Q, & \text{if } \phi' = w' \\[3mm]
\rho_0\left[N^2(fq' + F_\delta) + \dfrac{g}{c_p T_0}\dfrac{D}{Dt}\dfrac{\partial Q}{\partial z}\right], & \text{if } \phi' = p' \\[3mm]
\dfrac{N^2\theta_0}{g}\left(f\dfrac{\partial q'}{\partial z} + \dfrac{\partial F_\delta}{\partial z}\right) + \dfrac{\theta_0}{c_p T_0}\dfrac{D}{Dt}\dfrac{\partial^2 Q}{\partial z^2}, & \text{if } \phi' = \theta'.
\end{cases}
\tag{10}
$$

In (10), $F_\delta = \partial F_x/\partial x + \partial F_y/\partial y$ is the *divergence* associated with the momentum forcing (e.g., Zhu and Holton 1987). A mathematically closed system consists of the potential vorticity equation (6) and one of the wave equations from (8). This system requires the specification of the three initial conditions ϕ_i', $\partial\phi_i'/\partial t$, and q_i'. In order to investigate the adjustment dynamics of a nonresting continuously stratified atmosphere, the geostrophic degeneracy of the f-plane equations (e.g., Gill 1982; Pedlosky 1987) must be lifted by determining the spatial distribution of the linearized PV as a function of time by solving (6). Once this distribution is obtained, it can be incorporated into the right side of the linearized wave equations from which the respective dynamical fields $\mathbf{u}'$, p', and θ' can be obtained.

Because q' is conserved in the moving coordinates with $\mathbf{U} = U\mathbf{i} + V\mathbf{j}$ in the absence of external forcing, the perturbation PV (q' term) on the right side of each component equation (8) is related to the steady part of the variable on the left side. When $D/Dt = 0$ in (9) and $F_x(\mathbf{r}, t) = F_y(\mathbf{r}, t) = Q(\mathbf{r}, t) = 0$ in (10), each component equation of (8) reduces to an elliptical equation that governs the steady-state part of the solution. These elliptical equations manifest the invertability of the final q' because, in general, q' is not invertable *until the perturbation fields reach thermal wind balance*. Thus the perturbation PV theory developed here is essentially a method of partitioning the solution into two parts, (i) a purely transient part obtained from (8) and (9) with $F_x(\mathbf{r}, t) = F_y(\mathbf{r}, t) = Q(\mathbf{r}, t) = q'(\mathbf{r}, t) = 0$, and (ii) a steady-state part obtained from (8) and (9) with $F_x(\mathbf{r}, t) = F_y(\mathbf{r}, t) = Q(\mathbf{r}, t) = 0$ and $D/Dt = 0$ (which corresponds to $t \to \infty$).

b. The initial-value problem

For a vertically unbounded Boussinesq atmosphere, we can define the three-dimensional Fourier transform of any field variable and its inverse by the integral pair

$$
\hat{\phi}(\mathbf{k}, t) = \frac{1}{(2\pi)^3}\int_{-\infty}^{\infty}\int_{-\infty}^{\infty}\int_{-\infty}^{\infty}\phi'(\mathbf{r}, t)e^{-i\mathbf{k}\cdot\mathbf{r}}\,d\mathbf{r}, \tag{11}
$$

$$
\phi'(\mathbf{r}, t) = \int_{-\infty}^{\infty}\int_{-\infty}^{\infty}\int_{-\infty}^{\infty}\hat{\phi}(\mathbf{k}, t)e^{i\mathbf{k}\cdot\mathbf{r}}\,d\mathbf{k}, \tag{12}
$$

where $\mathbf{k} = (k, l, m)$. Taking the Fourier transform of the potential vorticity equation in the absence of any thermal or mechanical forcing yields

$$
\frac{\partial\hat{q}}{\partial t} + i(kU + lV)\hat{q} = 0. \tag{13}
$$

Equation (13) has the following general solution:

$$
\hat{q}(\mathbf{k}, t) = \hat{q}_i(\mathbf{k})e^{-i\Omega t}, \tag{14}
$$

where $\Omega = kU + lV$ is the intrinsic wave frequency and q_i is the initial perturbation potential vorticity distribution. With the addition of a nonzero basic-state flow, the PV distribution associated with the initial disturbance is advected downstream from its initial location. The Fourier transform of the initial potential vorticity (7) is

$$
\hat{q}_i(\mathbf{k}) = i[k\hat{v}_i(\mathbf{k}) - l\hat{u}_i(\mathbf{k})] - \frac{m^2 f}{\rho_0 N^2}\hat{p}_i(\mathbf{k}), \tag{15}
$$

where the subscript i denotes the initial disturbance and m is the vertical wavenumber.

Expanding the material derivative and taking the Fourier transform of the inhomogeneous wave equations (8), (9), and (10) with $F_x(\mathbf{r}, t) = F_y(\mathbf{r}, t) = Q(\mathbf{r}, t) = 0$ yields

$$
\frac{\partial^2\hat{\phi}}{\partial t^2} + 2i\Omega\frac{\partial\hat{\phi}}{\partial t} + \left(\frac{N^2\kappa^2}{m^2} + f^2 - \Omega^2\right)\hat{\phi} = R(\mathbf{k})e^{-i\Omega t}. \tag{16}
$$

In (16), $\kappa^2 = k^2 + l^2$. The coefficients $R(\mathbf{k})$ for each variable $\phi' = (\mathbf{u}', p', \text{ or } \theta')$ can be found in the appendix. Primary contributions to the complete Fourier spectrum of zonal, meridional, and vertical wavenumbers, defined here as $k = 2\pi/a_x$, $l = 2\pi/a_y$, and $m =$
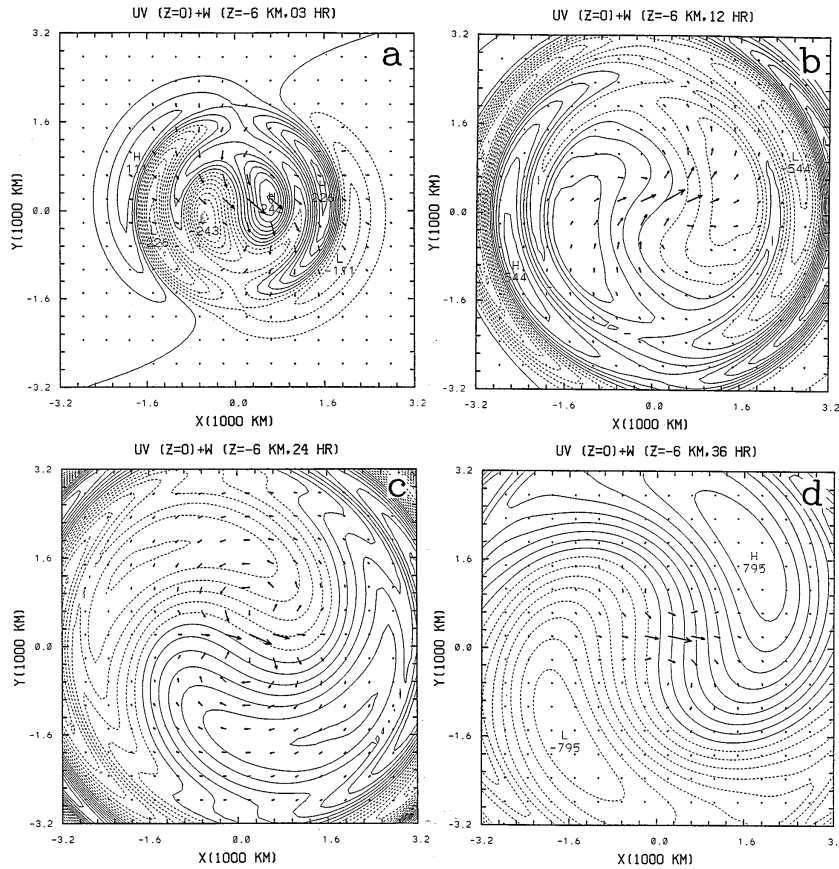
FIG. 1. Linear solution for $\mathbf{V}' = u\mathbf{i} + v'\mathbf{j}$ at $z = 0$ superimposed on vertical motion w' at $z = -6$ km at (a) $t = 3$ h, (b) $t = 12$ h, (c) $t = 24$ h, and (d) $t = 36$ h produced by the impulsive addition of zonally localized momentum from an unbalanced jet given by (18) to a quiescent, rotating, unbounded, continuously stratified Boussinesq atmosphere. The jet and flow parameters are $u_{j0} = 20$ m s^{-1}, $a = b = 500$ km, $d_{\text{jet}} = 12.5$ km, $N = 10^{-2}$ s^{-1}, and $f = 10^{-4}$ s^{-1}.

$2\pi/a_z$, will come from an initial disturbance whose zonal, meridional, and vertical scales are a_x, a_y, and a_z, respectively. The general solution to the perturbation potential vorticity equation (14) has been incorporated into the inhomogeneous source terms on the right-hand side of (16). The wave equations (16) have a general solution of the form

$$\hat{\phi}(\mathbf{k}, t) = A_\phi(\mathbf{k})e^{+i\omega_- t} + B_\phi(\mathbf{k})e^{-i\omega_+ t}$$

$$+ \frac{m^2 R(\mathbf{k})}{(N^2\kappa^2 + m^2 f^2)}e^{-i\Omega t}. \qquad (17)$$

The first two terms on the right-hand side correspond to the transient inertia–gravity waves excited by the nonzero divergence tendency of the *ageostrophic* wind field associated with the initial perturbation PV distribution. The third term corresponds to the linear, geostrophically balanced, steady-state equilibrium (which is advected downstream) that the initial ageostrophic potential vorticity state asymptotically approaches. The dispersion relationship of the transient inertia–gravity waves is given in the appendix. The downstream advection of the

balanced equilibrium state does not excite any further inertia-gravity wave modes because it does not possess a propagation speed that is different from the advection speed of the basic state flow.

The remaining unknown coefficients represented by $A_\phi(\mathbf{k})$ and $B_\phi(\mathbf{k})$ are determined by imposing the appropriate initial conditions $\mathbf{u}_i'$, p_i', θ_i', $\partial\mathbf{u}_i'/\partial t$, $\partial p_i'/\partial t$, and $\partial\theta_i'/\partial t$. Recall that each system consisting of one wave equation (8) and the potential vorticity equation (6) requires the three initial conditions ϕ_i', $\partial\phi_i'/\partial t$, and q_i' for a unique solution. Because we are interested in the adjustment to geostrophic equilibrium from the ageostrophic initial state characterized by an unbalanced zonal wind anomaly, we take our set of initial conditions to be

$$u_i'(\mathbf{r}) = u_{\text{jet}}(\mathbf{r}) = u_{j0}(x^2/a^2 + y^2/b^2 + 1)^{-3/2}e^{-z^2/d_{\text{jet}}^2} \qquad (18)$$

$$v_i'(\mathbf{r}) = p_i'(\mathbf{r}) = \theta_i'(\mathbf{r}) = 0. \qquad (19)$$

Initial conditions for w', $\partial\mathbf{u}'/\partial t$, $\partial p'/\partial t$, and $\partial\theta'/\partial t$ can be found in the appendix. For the particular problem addressed here, an unbalanced zonal wind anomaly in a rotating continuously stratified atmosphere is equiv-

U (X,Y=0,Z,T=3 HR)   U (X,Y=0,Z,T=12 HR)

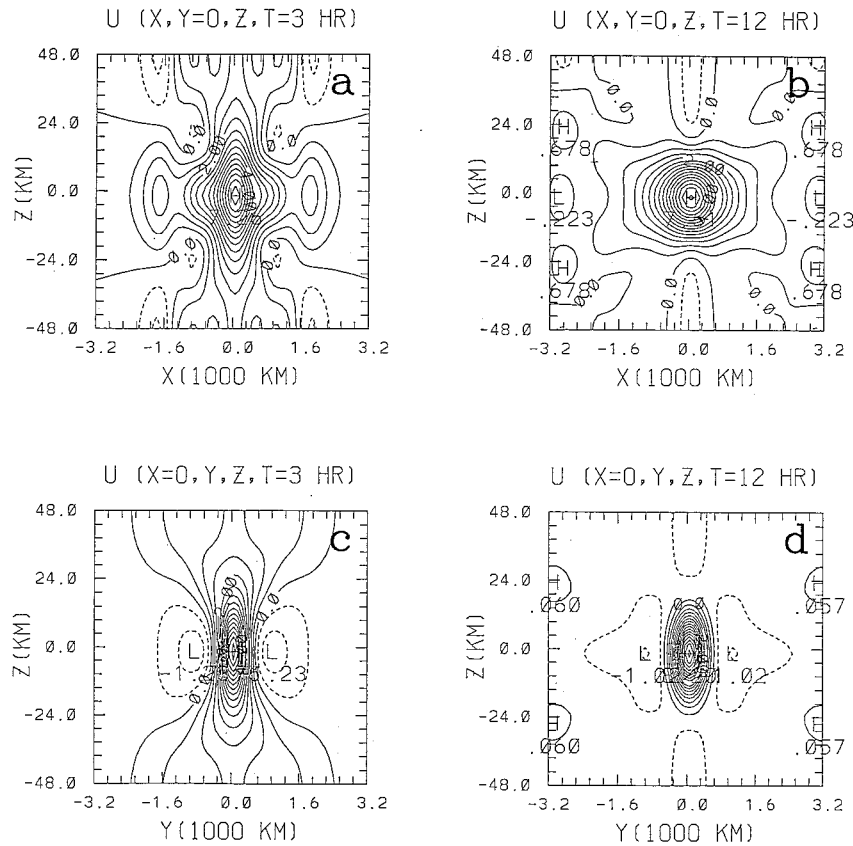U (X=0,Y,Z,T=3 HR)   U (X=0,Y,Z,T=12 HR)

Fig. 2. East–west (a, b) and north–south (c, d) vertical cross sections of u' at (a) $t = 3$ h, (b) $t = 12$ h, (c) $t = 3$ h, and (d) $t = 12$ h. The contour interval for all panels is 0.5 m s^{-1}.

alent to a perturbation PV distribution given by the meridional gradient of the ageostrophic jet,

$$q'_i(\mathbf{r}) = -\frac{\partial u_{\text{jet}}}{\partial y}(\mathbf{r}). \qquad (20)$$

This PV distribution takes the form of a *dipole,* characterized by an isolated positive (negative) PV anomaly north (south) of the jet core, and defines the appropriate initial condition on the perturbation potential vorticity which is required for a unique solution. Equation (18) and the definition of q' from (7) have been used to derive (20).

The Fourier transform of (20) is used in (A1), which determines the coefficient for the geostrophically balanced equilibrium (third) term on the right-hand side of the general solution given by (17). The other coefficients $A(\mathbf{k})$ and $B(\mathbf{k})$ are listed in the appendix. The solution in physical space is then obtained by integrating (12) numerically through the use of a fast Fourier transform (FFT) algorithm.

c. Transient dynamics in the development of a geostrophically balanced jet streak

Figure 1 shows the response in the wind fields predicted by linear theory during the first 36 h after the

unbalanced zonal wind anomaly given by (18) is introduced into a quiescent, unbounded, stably stratified, Boussinesq atmosphere. The basic-state flow parameters are taken to be $N = 0.01$ s^{-1}, $f = 10^{-4}$ s^{-1}, $\rho_0 = 1$ kg m^{-3}, and $\theta_0 = 273$ K. The magnitude of the initial zonal wind anomaly is $u_{j0} = 20$ m s^{-1}, and its zonal and meridional half-widths and vertical e-folding scale are specified to be $a = b = 500$ km and $d = 12.5$ km, respectively. It should be noted that $d,$ the depth scale of our initial momentum perturbation, is a significant fraction of (slightly greater than) the typical scale height of the troposphere ($\sim$10 km). For such a deep perturbation, an anelastic rather than Boussinesq approximation [similar to that adopted by Walterscheid and Boucher (1984) and Zhu and Holton (1987)] is necessary to rigorously address the linear geostrophic adjustments associated with deep impulsive forcing. However, a Boussinesq approximation is adopted here in order to be able to compare our results directly with those appearing in the recent literature (e.g., Luo and Fritts 1993), in addition to yielding a fairly large deformation radius such that the perturbation mass fields adjust to this initial disturbance in the zonal wind field. Although there exists an infinite number of Rossby deformation radii in a continuously stratified atmosphere [see
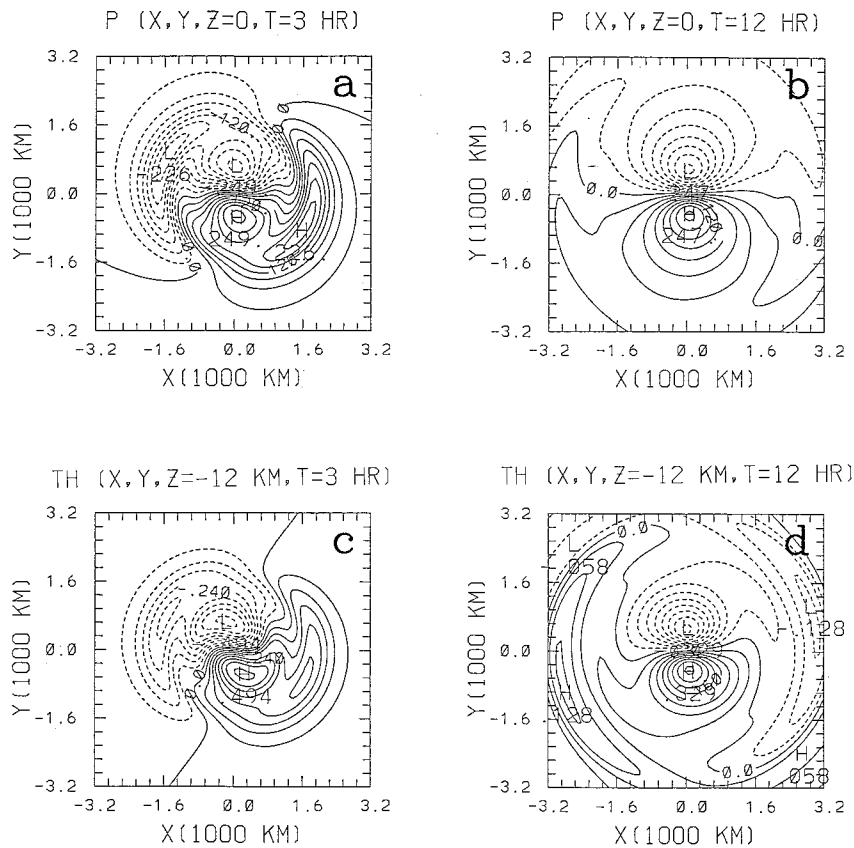
FIG. 3. Same as Fig. 1 except that p' at $z = 0$ and θ' at $z = -12$ km are shown. The contour interval for (a) and (b) is 0.3 mb, (c) 0.06 K, and (d) 0.04 K.

(A2)], the parameter $L_R = NH/f$, where H is the total depth of the initial disturbance ($2d_{jet}$), is the dominative horizontal scale (e.g., Blumen 1972; Gill 1982) that determines the relative importance of the Coriolis force compared to the gravitational restoring force. For example, $H = 2d_{jet} = 25$ km yields an L_R of 2500 km. If a and b are taken to be 500 km ($=L_R/5$), an initial disturbance of this horizontal and vertical scale in a continuously stratified atmosphere will tend to evoke a response in which the mass fields (p', θ') adjust to an initial perturbation in the wind field. In Fig. 1, the vertical motion w' at $z = -6$ km (i.e., 6 km below the jet core) is superimposed on the perturbation vector winds at $z = 0$.

By $t = 3$ h (Fig. 1a), a zonally localized, NW–SE oriented jet streak exists in the vicinity of the initial zonal wind anomaly and has a maximum magnitude of 10.5 m s^{-1}. Two isolated cells in w' that characterize ascent/descent in the jet streak exit/entrance region exist on the $z = -6$ km plane of 2.43×10^{-2} m s^{-1} magnitude and are flanked by radially propagating inertia–gravity waves (IGWs) to the east and west. These transient gravity waves are 180° out of phase, and have magnitudes of 2.26×10^{-2} m s^{-1} and 1.11×10^{-2} m s^{-1}, respectively. These two modes have zonal propagation speeds of $c_{px} \sim 148$ and 178 m s^{-1}, respectively. Because the

response is inviscid, these transient IGWs will, on a spherical earth, definitely be influenced by the β effect and return to their midlatitude source region in about 2 days. However, we are interested here in the near field, long-term asymptotic geostrophic and ageostrophic perturbation fields as the initially unbalanced zonal wind anomaly evolves into a zonally localized jet streak. We assume that once the transient IGWs propagate to the far field, they can no longer influence the evolution in the vicinity of the source region. It can be inferred from Fig. 1a that the NW–SE orientation of $\mathbf{V}' = u'\mathbf{i} + v'\mathbf{j}$ indicates that $u' > 0$ and $v' < 0$ near $\mathbf{r} = (0, 0, 0)$. A well-defined, localized, positive zonal wind anomaly of ~ 8.09 m s^{-1} is centered at the origin (not shown). This localized region of $u' > 0$ on the $z = 0$ plane is flanked to the north and south by localized regions of negative u' with magnitudes of 1.28 m s^{-1}. These negative zonal wind perturbations are supported by evolving high–low pressure perturbations (Fig. 3a). The v' field on the $z = 0$ plane at this time exhibits a localized northerly perturbation of 6.70 m s^{-1} and is primarily responsible for the orientation of $\mathbf{V}'$ shown in Fig. 1a. This perturbation flow component is excited by the meridional acceleration generated by the Coriolis force acting on
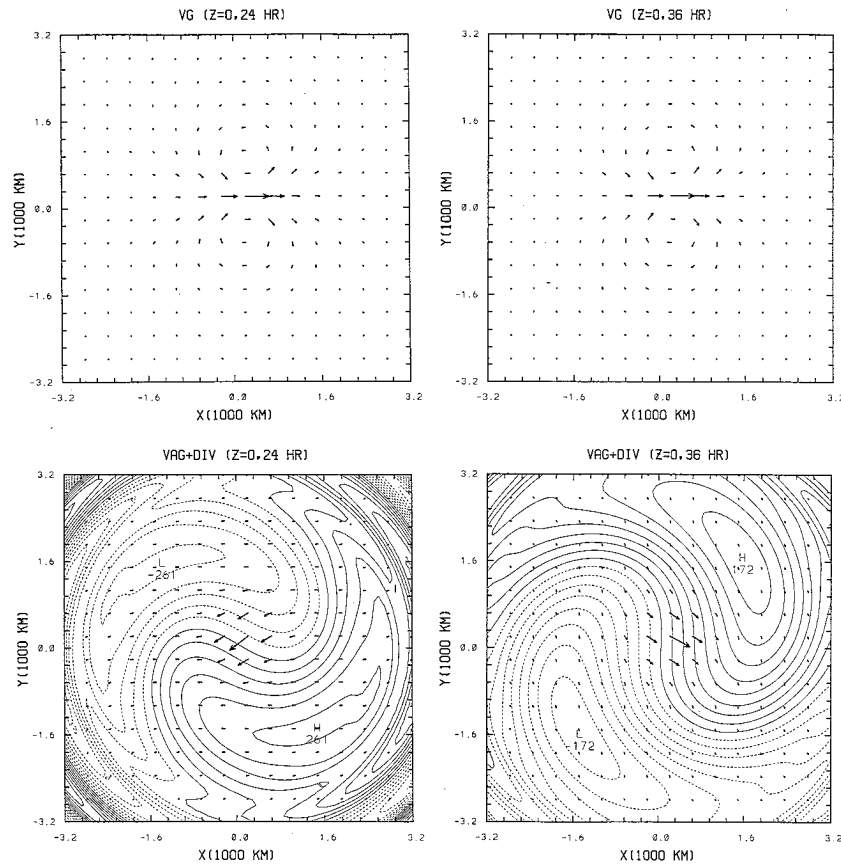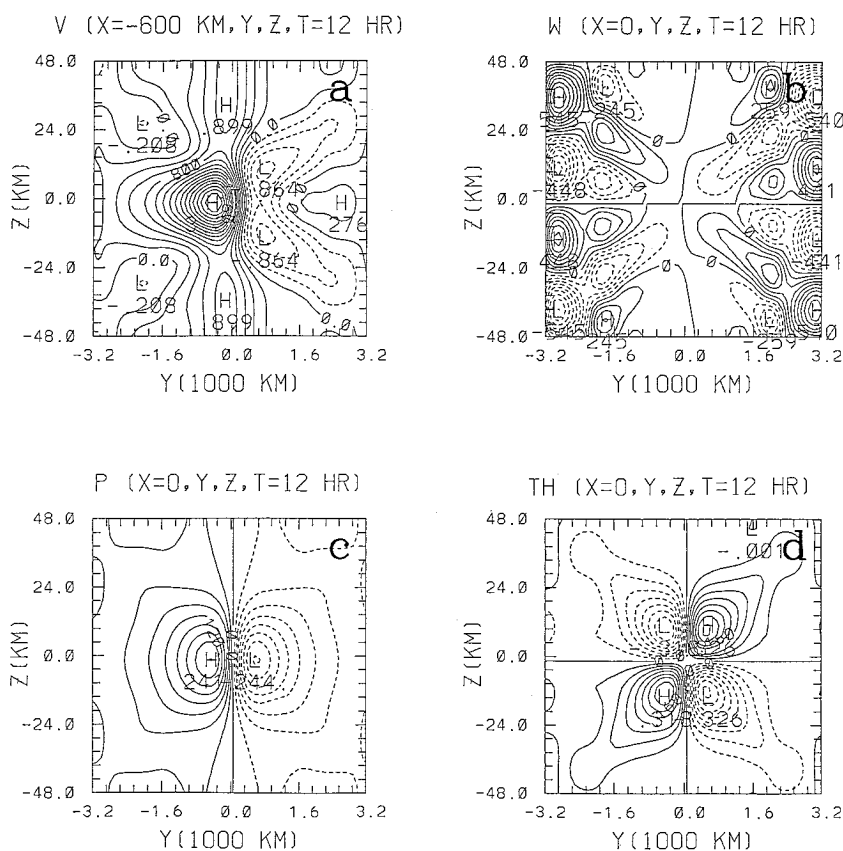
FIG. 4. Geostrophic perturbation vector winds (a), (b) and ageostrophic perturbation vector winds superimposed on horizontal divergence fields (c), (d) at $t = 24$ and 36 h.

the unbalanced zonal wind anomaly at $t = 0$ through the initial condition imposed by (A6).

At $t = 12$ h, the jet streak is oriented in a SW–NE direction and the total perturbation wind ($\mathbf{V}'$) has a magnitude of 9.76 m s^{-1} (Fig. 1b). Confluence/diffluence exists in the jet streak entrance/exit region. The cyclonic rotation of $\mathbf{V}'$ from $t = 3$ h is due to an inertial oscillation that has a period, $2\pi/f$ ($\sim$18 h), experienced by the meridional wind perturbation v'. Because the group velocity associated with this component of the response to geostrophic equilibrium is nearly zero (e.g., Gill 1982), it will take several inertial periods before the fluid in the vicinity of the source region reaches equilibrium. Dispersion will gradually take place as the longer wavelength components comprising the complete Fourier spectrum of the unbalanced initial state are slowly radiated to the far field. This is evident from the temporal evolution as discussed below. Centers of transient IGWs of 9.0×10^{-3} m s^{-1} on the $z = -6$-km plane have propagated to $x = \pm 3200$ km by this time, while other centers of 5.44×10^{-3} m s^{-1} are located at $x = \pm 2560$ km. The zonal phase speeds of these modes are $c_{px} = 74$ m s^{-1} and 59.26 m s^{-1}, respectively. At this time, a well-developed positive zonal wind anomaly of 8.41 m s^{-1} is centered at the origin on the $z = 0$

plane and is flanked by isolated regions of 1.06 m s^{-1} negative perturbation winds (not shown). The v' field consists of a southerly perturbation of 5.69 m s^{-1}, which exists in the NW and SE quadrants and flanks the jet core (not shown). This evolving horizontal structure in v' indicates the formation of confluence/diffluence in the jet streak entrance/exit region.

Figures 1c and 1d show $\mathbf{V}'$ at $z = 0$ superimposed on w' at $z = -6$ km at $t = 24$ and 36 h, respectively. Although the jet streak still has a slight NW–SE orientation at $t = 24$ h (Fig. 1c), the deviation from a zonally oriented east–west direction is substantially less than that at $t = 3$ h (Fig. 1a). This indicates that the amplitude of the inertial oscillation of v' at the origin has been reduced and that the ageostrophic divergence of the evolving perturbation flow field is effectively dispersed by radially propagating, transient IGWs into the far field. Rather significant cyclonic and anticyclonic circulations flank the core of the isolated jet streak at this time (Fig. 1c), and are associated with the strengthening negative zonal wind perturbations ($u' < 0$) that formed earlier in the adjustment process. The centers of these circulations are located roughly 640 km north and south of $y = 0$, and have been displaced closer to the axis of the jet core as $|\partial u'/\partial y|$ increases as the initially
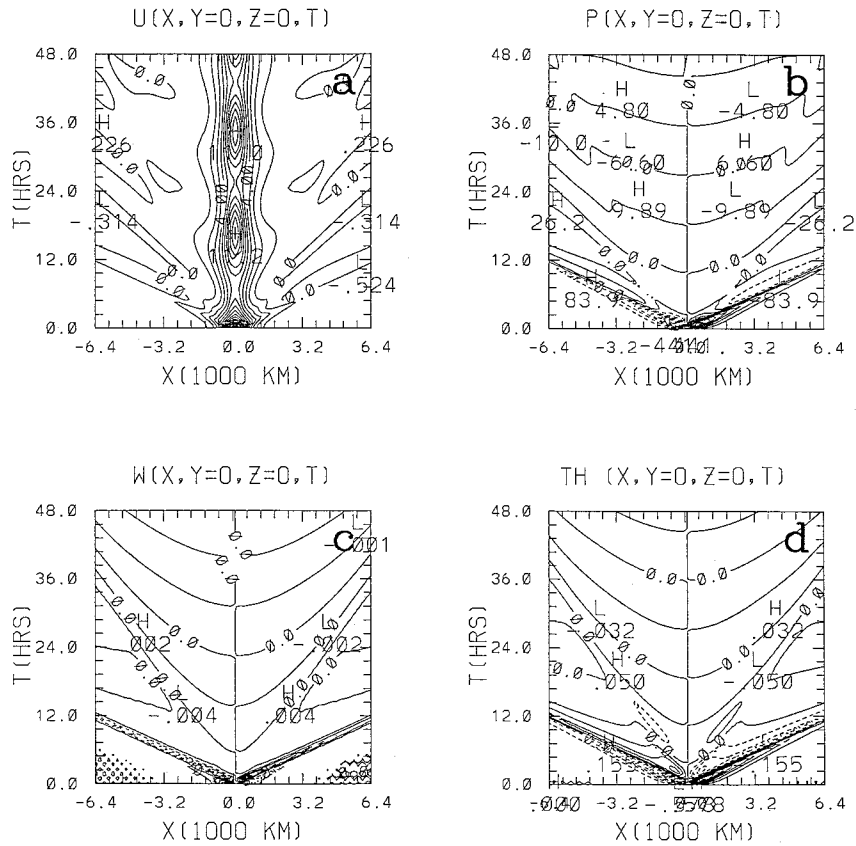
FIG. 5. North–south vertical cross sections of (a) v' at 600 km west of the main jet core, (b) w', (c) p', and (d) θ' at $x = 0$ at $t = 12$ h. The contour intervals for (a)–(d) are, respectively, 0.2 m s^{-1}, 6.0 × 10^{-4} m s^{-1}, 0.3 mb, and 0.04 K.

circular ($a = b = 500$ km), unbalanced zonal wind anomaly evolves into a geostrophically balanced, zonally elongated jet streak. By $t = 36$ h, $\mathbf{V}'$ (Fig. 1d) shows an isolated, primarily zonally oriented meso-α-scale jet streak of 10.8 m s^{-1}, whose length and width are approximately 1920 and 640 km, respectively. Also evident in the w' field is the fact that longwave transient IGWs continue to propagate out from the source region and slowly disperse into the surrounding fluid, which allows the source region to asymptotically approach geostrophic equilibrium.

Figures 2a and 2b show the east–west vertical cross section through $y = 0$ of u' at $t = 3$ and 12 h. Early in the adjustment at $t = 1$ h (not shown), the wind anomaly is primarily confined to within an e-folding distance of $\mathbf{r} = (0, 0, 0)$. Two hours later at $t = 3$ h (Fig. 2a), two horizontally propagating IGW modes whose centers are located at $x \sim \pm 1600$ km are present. By $t = 12$ h, most of the significant transient IGW activity at this location has virtually ceased, yielding a well-defined, vertically isolated zonal wind perturbation with the maximum of ~ 7.6 m s^{-1} (Fig. 2b).

Figures 2c and 2d show the north–south vertical cross section through $x = 0$ of u' at $t = 3$ and 12 h. Similar to the x–z cross section, the y–z cross section at $t = 1$ h shows that the zonal wind anomaly is vertically confined to within an e-folding distance of the origin (not shown). Two hours later at $t = 3$ h, the negative zonal wind perturbations (where $u' < 0$) have already formed (Fig. 2c). The magnitude of the zonal wind perturbations has strengthened almost by a factor of 3 by $t = 6$ h, while the magnitude of the primary zonal jet core reduces by ~ 2 m s^{-1} (not shown). During the subsequent 6-h period, the magnitude of the zonal wind anomaly strengthens by ~ 3 m s^{-1} (Fig. 2d), while the negative zonal wind perturbations decrease in magnitude, indicating that u' is still asymptotically adjusting to its final equilibrium value, which conserves the perturbation PV associated with the initial disturbance.

Figure 3 shows horizontal cross sections of the p' and θ' fields at $z = 0$ and -12 km, respectively. The present linear theory predicts that the hydrostatically balanced mass fields quickly adjust to the initial perturbation wind field, leaving couplets of low–high perturbation pressure (Figs. 3a and 3b) and cold–warm air (Figs. 3c and 3d) north/south of the origin at all levels below the level of maximum zonal perturbation wind (Figs. 7c and 7d). The θ' fields are reversed at all levels above $z = 0$ (Fig. 7d)

FIG. 6. Temporal evolution of (a) u', (b) p', (c) w', and (d) θ' in the zonal direction at $y = 0$ during the first 48 h for the initial-value problem. The contour intervals for (a)–(d) are, respectively, 1.0 m s^{-1}, 0.50 mb, 0.02 m s^{-1}, and 0.07 K.

and, in the absence of any vertical motions (i.e., as $t \rightarrow \infty$), therefore maintain a local *linear thermal wind balance* between the three-dimensional baroclinic perturbations.

Figure 4 shows the perturbation geostrophic vector winds $\mathbf{V}'_g = u'_g \mathbf{i} + v'_g \mathbf{j}$, and the divergence $\delta = \partial u'_a / \partial x + \partial v'_a / \partial y$ superimposed on the perturbation ageostrophic vector winds $\mathbf{V}'_a = u'_a \mathbf{i} + v'_a \mathbf{j}$ at $t = 24$ and 36 h. Although longwave IGWs are still slowly propagating out from the source region (Figs. 4c and 4d), space–time cross sections (Fig. 6) show that a majority of the transient, dispersive IGWs have propagated far from the origin during the first 12 h. Therefore, a partitioning of the zonal (u') and meridional (v') wind perturbations into geostrophic and ageostrophic ($u'_a = u' - u'_g$, $v'_a = v' - \theta v'_g$) components for $t \geq 12$ h is permissible. This is not possible when the transient IGWs are still in the near field, since p' includes both geostrophic and ageostrophic components.

Figure 4a shows that a significant geostrophic zonal jet has formed in the vicinity of the origin by $t = 24$ h, whose geometry and orientation change little for all times greater than this (Fig. 4b). The length/width of this geostrophic jet is approximately 2240 km/640 km, and is flanked by a cyclonic/anticyclonic circulation, roughly 960 km in diameter north/south of the jet core.

The magnitude of this geostrophic jet at $t = 24$ h is 10.2 m s^{-1}, which reduces to 6.44 m s^{-1} by $t = 36$ h. This component of the perturbation flow is due to the horizontal gradients in the high–low perturbation pressure couplet (Fig. 3b) that has formed as the perturbation mass field quickly adjusts to the sub-Rossby-scale disturbance in the initial wind (i.e., $a \ll L_R$) and is consistent with results of classical shallow water adjustment theory (e.g., Rossby 1938; Cahn 1945; Blumen 1972), and the recent 3D linear stratified theory of Luo and Fritts (1993). Rather significant ageostrophic components of $\mathbf{V}'$ still exist at $t = 24$ h and 36 h (Figs. 4c and 4d). The ageostrophic flow is oriented in the NE–SW direction and has a magnitude of 4.73 m s^{-1} at $t = 24$ h. Again, this is associated with an inertial oscillation at the jet core. This ageostrophic flow becomes NW–SE oriented and has a magnitude of 4.68 m s^{-1} by $t = 36$ h. This ageostrophic perturbation wind decreases to zero as longwave transient IGWs gradually disperse into the far field.

Figure 5 shows y–z cross sections of v', w', p', and θ' at $t = 12$ h. Six hundred kilometers to the west of the main jet core, an isolated cell of $v' > 0$ of $\sim$3.2 m s^{-1} exists on the south side in the jet entrance region (Fig. 5a). Above and below $z = 0$, north of $y = 0$,
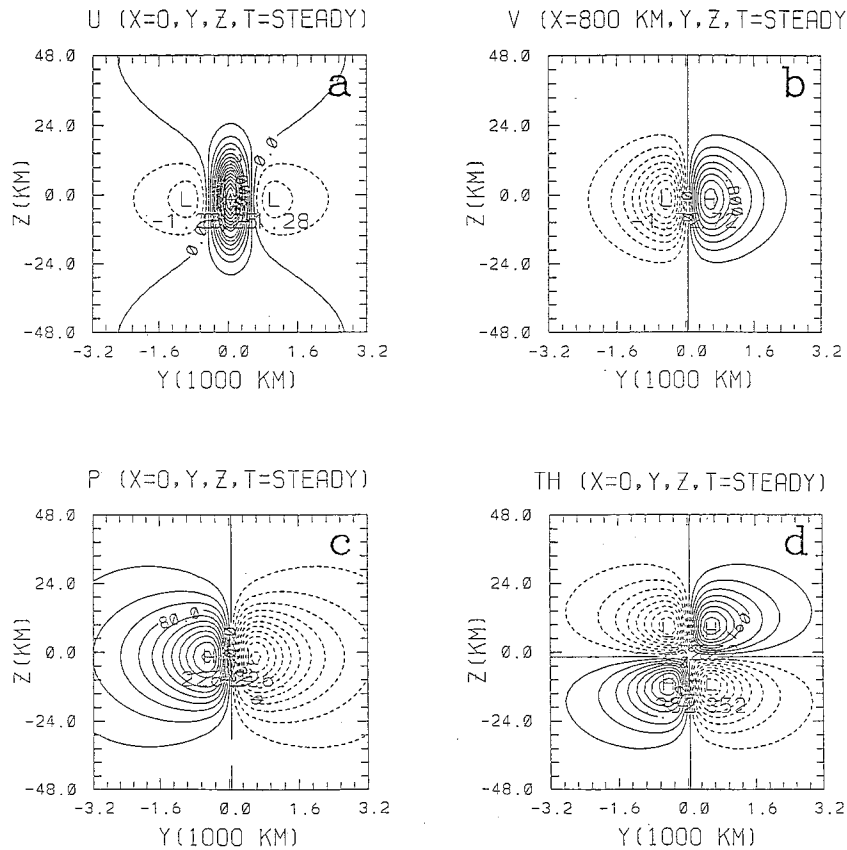
FIG. 7. North–south vertical cross sections of (a) u', (b) v' at 800 km east of the jet core in the exit region, (c) p', and (d) θ' of the linear, steady-state response to the localized ageostrophic momentum. The contour intervals for (a)–(d) are, respectively, 0.50 m s^{-1}, 0.20 m s^{-1}, 0.20 mb, and 0.04 K.

vertically propagating IGWs are clearly evident in the v' field. On the $x = 0$ plane, above and below $z = 0$, transient, vertically propagating IGWs (clearly evident in w') are dispersing ageostrophic wave energy into the surrounding atmosphere as the fluid approaches a new balanced equilibrium (Fig. 5b). Figures 5c and 5d show that isolated couplets of perturbation high–low pressure are colocated with warm/cold air on the south/north side of the zonal jet below $z = 0$. This pattern is reversed above $z = 0$, as required by the hydrostatic balance.

Figure 6 shows the temporal evolution in u', p', w', and θ' at $(x, 0, 0)$ predicted by linear theory during the first 48 h of adjustment. Figure 6a shows that u' decreases steadily during the early stages of adjustment, reaching a minimum of ~6 m s^{-1} at $t \sim 7.5$ h, after which it begins to increase and approach another maximum of approximately 11.2 m s^{-1} at $t \sim 17$ h. The zonal wind perturbation u' continues to oscillate about its final equilibrium value with slowly decreasing ampltitude for all time after this. The negative zonal perturbation winds ($u' < 0$) flanking the jet core begin forming at $t \sim 3$ h and continue to evolve with maxima forming at $y \sim \pm 960$ km approximately at $t \sim 6$ h (not shown). This portion of the perturbation return flow

occurs at approximately the same time as the high–low couplet in p' reaches its maximum value. The zonal wind anomaly with its compensating counter currents continually oscillates about its final equilibrium value for $t > 12$ h (Fig. 6a). Most of the transient IGW activity propagating in the zonal direction associated with the evolving p' field (not shown) occurs during the first 12 h of the adjustment. These IGWs propagate a distance of $|x| \sim 6400$ km during this time, yielding a zonal phase speed of $c_{px} \sim 148$ m s^{-1}.

Detailed analysis of the temporal evolution in w' and θ' fields (Figs. 6c and 6d) indicate that a broader spectrum of wave modes are excited in the zonal direction during the first 12 h of adjustment, in which there are at least three primary modes evident in w' (not shown). The first mode originates at $t = 0$ and has a zonal propagation speed of $c_{px} \sim 148$ m s^{-1}. The second and third modes originate at $t \sim 1.2$ h. The second mode has a phase speed of $c_{px} \sim 185$ m s^{-1}, while the third mode has a phase speed of $c_{px} \sim 82.3$ m s^{-1}. Figure 6c shows that most of the transient zonal IGW activity associated with w' is essentially dispersed during the first 12 h. Further detailed analysis (not shown) indicates that there are two primary IGW modes embedded within the pos-
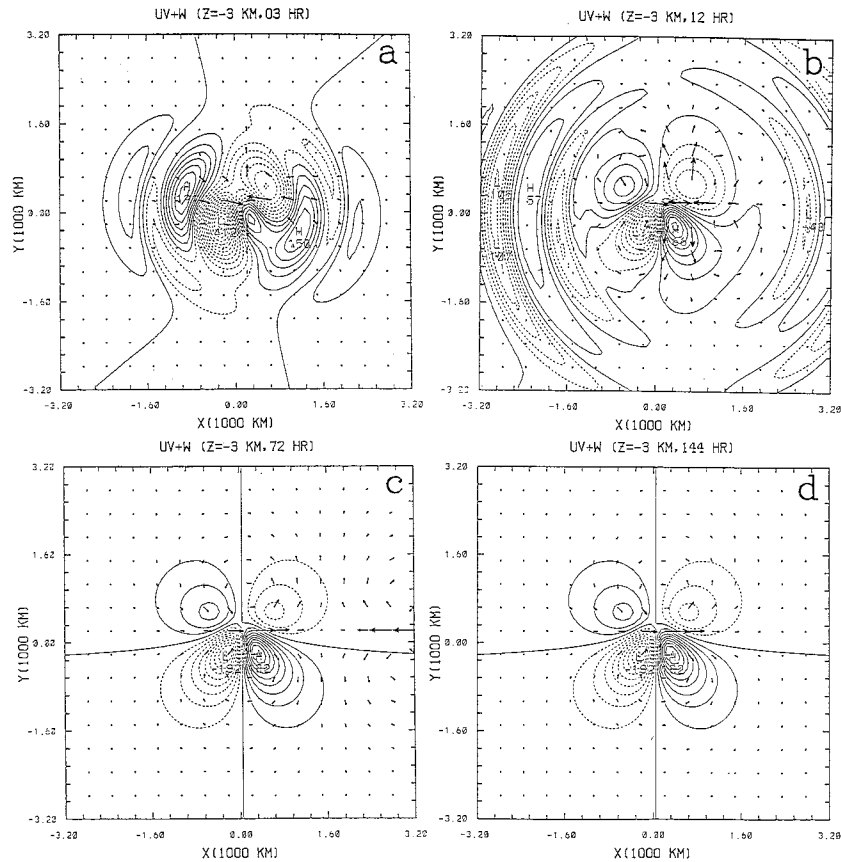
FIG. 8. Same as Fig. 1 except at (a) $t = 3$ h, (b) $t = 12$ h, (c) $t = 72$ h, and (d) $t = 144$ h in the frame of reference moving at the speed $c = 10$ m s^{-1} due to the imposed steady momentum forcing given by Eq. (21). Flow parameters are the same as in Fig. 1 except $U = 20$ m s^{-1} and $u_{j0} = 30$ m s^{-1}.

itive (negative) θ' modes east (west) of the origin (Fig. 6d). The first mode and a slower mode have phase speeds of $c_{px} \sim 148$ m s^{-1} and 80.8 m s^{-1}, respectively. Figure 6d also shows that the transient zonal IGW activity associated with θ' is also dispersed during the first 12 h. Although the majority of significant transient meridional IGW activity in θ' is dispersed for $t \leq 12$ h, slower propagating modes continue to be excited for times greater than this, due to the slow dispersion of longer Fourier modes comprising the unbalanced ageostrophic initial state. Significant meridional IGW activity is also excited during the first 12 h for all perturbation fields except u', which tends to exhibit oscillation about its final equilibrium value (not shown).

Figure 7 shows the north–south vertical cross sections of u', v', p', and θ' associated with the steady-state part of the total solution predicted by linear theory [last term on the right side of (17)]. The asymptotic balanced equilibrium on the x–y plane at $z = 0$ and below can be inferred from earlier figures (e.g., Figs. 1d, 3b, and 3d). The vertical cross section shown here clearly shows the existence of an isolated geostrophic jet (Fig. 7a) with meridionally confluent/diffluent flow in its entrance/exit

region (Fig. 7b), in hydrostatic balance with the thermodynamic fields (Figs. 7c and 7d). This steady-state therefore exhibits a localized, *linear thermal wind balance* among the baroclinic perturbations, which is devoid of any *steady-state ageostrophic circulations.* With the addition of a nonzero basic-state flow (not shown), the response is essentially the same as that outlined above, except that the transient IGWs are Doppler shifted by the basic-state flow. In addition, the geostrophically balanced zonal jet shown here is advected downstream at the speed U, thereby establishing the mechanisms of perturbation geostrophic vorticity advection, $-\mathbf{U} \cdot \nabla \zeta_g'$, and horizontal temperature advection, $-\mathbf{U} \cdot \nabla \theta'$, associated with the traveling PV couplet that characterizes this thermally balanced zonal jet streak.

Although the linear theory developed here can correctly predict the *primary* (geostrophic) circulations associated with midlatitude meso-α- to synoptic-scale jet streaks, the important *secondary* (ageostrophic) circulations responsible for *maintaining* the steady-state thermal wind balance (e.g., Gill 1982; Holton 1992; Bluestein 1993) do not exist. This deficiency of the linear theory (e.g., Weglarz 1994) arises because the perturbation PV

(7) makes no *final* contribution to the ageostrophic wind perturbations and hence by mass continuity, w' [$= -\int (\partial u_a'/\partial x + \partial v_a'/\partial y)\, dz$]. This deficiency is addressed by investigating the jet streak–mean flow interaction mechanism of entrance/exit region acceleration/deceleration experienced by the basic-state flow due to prescribed zonal momentum forcing in the next section.

3. Linear theory for the forced problem

In this section we formulate a linear theory of an *independently propagating* zonal wind anomaly in a uniform, continuously stratified Bousinessq flow, by including a prescribed external momentum forcing term in the zonal momentum equation (1). The imposed momentum forcing is assumed to be

$$F_x(\mathbf{r}, t) = U^* \frac{\partial}{\partial x}\left[u_{j0}\left\{ \frac{(x - ct)^2}{a^2} + \frac{y^2}{b^2} + 1 \right\}^{-3/2} \right] e^{-z^2/d_{\text{jet}}^2}. \tag{21}$$

The above equation parameterizes *the nonlinear inertial advective entrance (exit) region acceleration (deceleration)* that occurs when the basic-state flow passes through the core of a slower moving ($c < U$) jet streak as it forms in the background synoptic-scale flow. In (21), u_{j0} is the forcing magnitude; a, b, and d_{jet} are the zonal and meridional half-widths and vertical e-folding depth, respectively; and c is the propagation speed of the momentum forcing. The relative velocity of the basic-state flow to the forcing is $U^* = U - c$. We have assumed uniform propagation in the zonal direction for mathematical convenience.

The governing equations of this forced adjustment problem are given by (1)–(5) with $F_y(\mathbf{r}, t) = Q(\mathbf{r}, t) = 0$. In order to make this linear problem mathematically tractable, we introduce a standard Galilean transformation such that the response is viewed from the moving frame of the uniformly translating momentum forcing.

After the transformation, the potential vorticity and wave equations may be written as

$$L_\xi \phi'(\xi, y, z, t) = G_\xi(q', F_\xi), \tag{22}$$

where

$$L_\xi = \begin{cases} \dfrac{\partial}{\partial t} + (U - c)\dfrac{\partial}{\partial \xi} + V\dfrac{\partial}{\partial y}, & \text{if } \phi' = q' \\[2ex] \left\{ \left[\dfrac{\partial}{\partial t} + (U - c)\dfrac{\partial}{\partial \xi} + V\dfrac{\partial}{\partial y} \right]^2 + f^2 \right\} \dfrac{\partial^2}{\partial z^2} + N^2 \nabla_\xi^2, & \text{if } \phi' = (\mathbf{u}', p', \text{ or } \theta'). \end{cases} \tag{23}$$

Assuming that the particular form of applied momentum forcing is known, a mathematically closed system for the forced geostrophic adjustment problem consists of the potential vorticity equation and any one of the wave equations, both of which are written collectively here as (22). This system also requires the specification of the initial conditions ϕ'_i, $\partial \phi'_i/\partial t$, and q'_i for a unique solution.

The general solution to the perturbation potential vorticity equation is given by

$$\hat{q}(\mathbf{k}, t) = \left[\hat{q}_i(\mathbf{k}) + \frac{1}{\Omega}\hat{F}_\xi(\mathbf{k}) \right] e^{-i\Omega t} - \frac{1}{\Omega}\hat{F}_\xi(\mathbf{k}), \tag{24}$$

where $\Omega = k(U - c) + lV$ is the intrinsic wave frequency. The first term on the right-hand side of (24) shows that not only does any *preexisting* PV anomaly get advected downstream at the relative velocity $U - c$, but that an additional PV anomaly generated by the meridional gradient of the vorticity associated with the prescribed momentum forcing is advected downstream as well. If this forcing is chosen such that its Fourier transform is given by

$$\hat{F}_\xi(\mathbf{k}) = -\frac{\Omega}{1}\hat{q}_i(\mathbf{k}), \tag{25}$$

then any preexisting initial PV anomaly is completely *destroyed*.

The last term on the right-hand side of (24) is the steady-state contribution to the perturbation potential vorticity field due to the momentum forcing. An observer in a nontranslating reference frame will see this steady-state PV distribution propagate downstream through the basic-state flow at the speed c. The forced circulations associated with this distribution will be those identified by this observer as those characteristic of the independently propagating zonal jet and, for a proper choice of prescribed forcing, will be representative of those found with midlatitude jet streaks in the real atmosphere.

The general solution to the Fourier transformed wave equations may be written as

$$\hat{\phi}(\mathbf{k}, t) = A_\phi(\mathbf{k})e^{+i\omega_- t} + B_\phi(\mathbf{k})e^{-i\omega_+ t}$$
$$+ C_\phi(\mathbf{k})e^{-i\Omega t} + D_\phi(\mathbf{k}). \tag{26}$$

The coefficients $A(\mathbf{k})$, $B(\mathbf{k})$, $C(\mathbf{k})$, and $D(\mathbf{k})$ are determined by the initial conditions (ϕ'_i, $\partial \phi'_i/\partial t$) and can be found in the appendix. For this particular choice of initial conditions, (A16)–(A18), $q'_i = 0$. The solution in physical space is obtained through inverse FFT of (12).
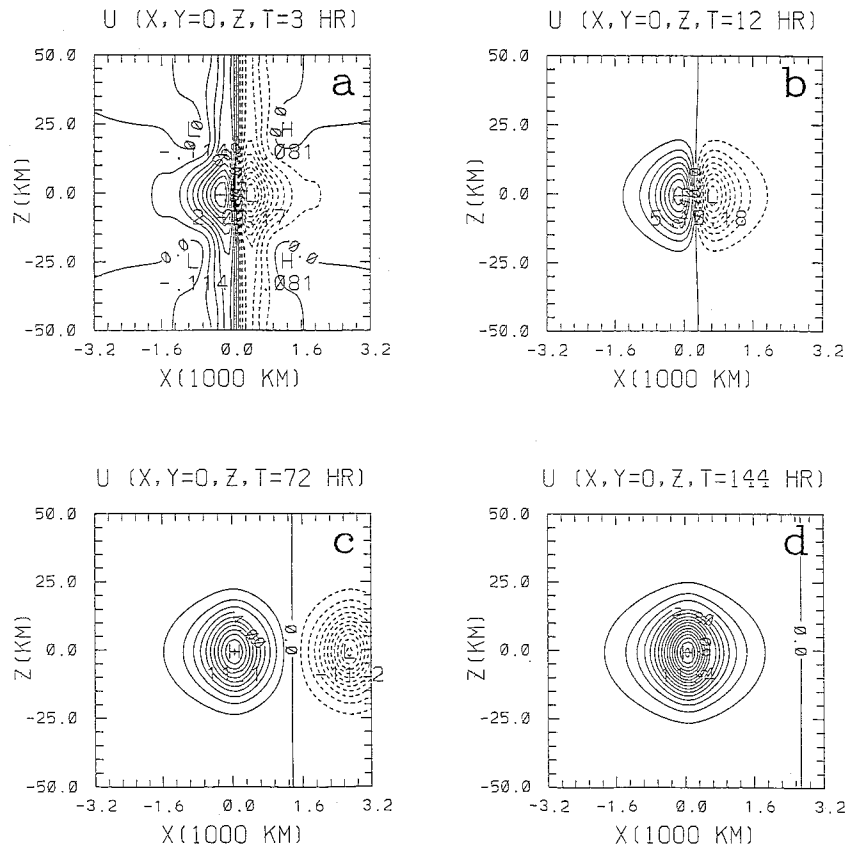
FIG. 9. Same as Fig. 2 except for the forced response at (a) $t = 3$ h, (b) $t = 12$ h, (c) $t = 72$ h, and (d) $t = 144$ h. The contour intervals for (a)–(d) are, respectively, 0.2 m s^{-1}, 0.60 m s^{-1}, 1.0 m s^{-1}, and 0.70 m s^{-1}.

Figures 8–15 show the horizontal and vertical cross sections of the forced baroclinic response in a moving frame of reference of $c = 10$ m s^{-1} in an unbounded, continuously stratified, Boussinesq atmosphere. The flow parameters are taken to be $N = 0.01$ s^{-1}, $f = 10^{-4}$ s^{-1}, $\rho_0 = 1$ kg m^{-3}, $\theta_0 = 273$ K, and $\mathbf{U} = (20, 0)$ m s^{-1}. The forcing parameters are $u_{j0} = 30$ m s^{-1}, $a = b = 500$ km, and $d = 12.5$ km. The Rossby number that characterizes the basic zonal flow may be estimated as $R_{o,U} = (U - c)/2af = 0.1$. Note that $|u_{j0}| > |U|$, but that $|c| < |U|$, yielding flow and propagation characteristics representative of midlatitude jet streaks (e.g., Bluestein 1993) embedded in large-scale flows.

Transient dynamics of the forced adjustment to quasigeostrophic jetogenesis

Figure 8 shows the evolution in $\mathbf{V}' = u'\mathbf{i} + v'\mathbf{j}$ at $z = 0$ (level of maximum forcing) superimposed on w' at $z = -3$ km. At $t = 3$ h (Fig. 8a), isolated easterly and westerly zonal jets form to the east and west of the forcing center, respectively, and are generated by acceleration/deceleration when the basic zonal flow passes through the forcing entrance/exit region. The maximum

zonal wind at this time is 2.45 m s^{-1}. These zonal wind components gradually strengthen (Fig. 8b) due to the steady forcing. By $t = 12$ h, $|u'_{max}|$ is 4.64 m s^{-1}. At this time, the center of the isolated westerly jet is roughly colocated with the forcing center, while the core of the easterly zonal jet has been advected 1280 km downstream. A pair of anticyclonic and cyclonic mesoscale circulations approximately 800 km in diameter are developing north and south of the easterly jet. An opposite pair of circulations is also associated with the westerly jet. The easterly zonal jet continues to be advected downstream at the relative velocity $U - c$, whose core is located roughly 3200 km downstream of the forcing center by $t = 72$ h (Fig. 8c), leaving in the vicinity of $\mathbf{r} = (0, 0, 0)$ a localized westerly zonal jet whose magnitude is 12.6 m s^{-1} by $t = 144$ h (Fig. 8d).

Figure 8 also shows the w' field on the $z = -3$ km plane. At $t = 3$ h, at least four centers of outwardly propagating IGWs both east and west of $\mathbf{r} = (0, 0, 0)$ can be identified (Fig. 8a). Two cells of rising motion are located at approximately $x = \pm 1920$ km. If these modes were excited at $t = 0$, their zonal phase speed must be approximately $c_{px} \sim 177.8$ m s^{-1}. The next pair of IGWs closest to the origin are associated with sinking
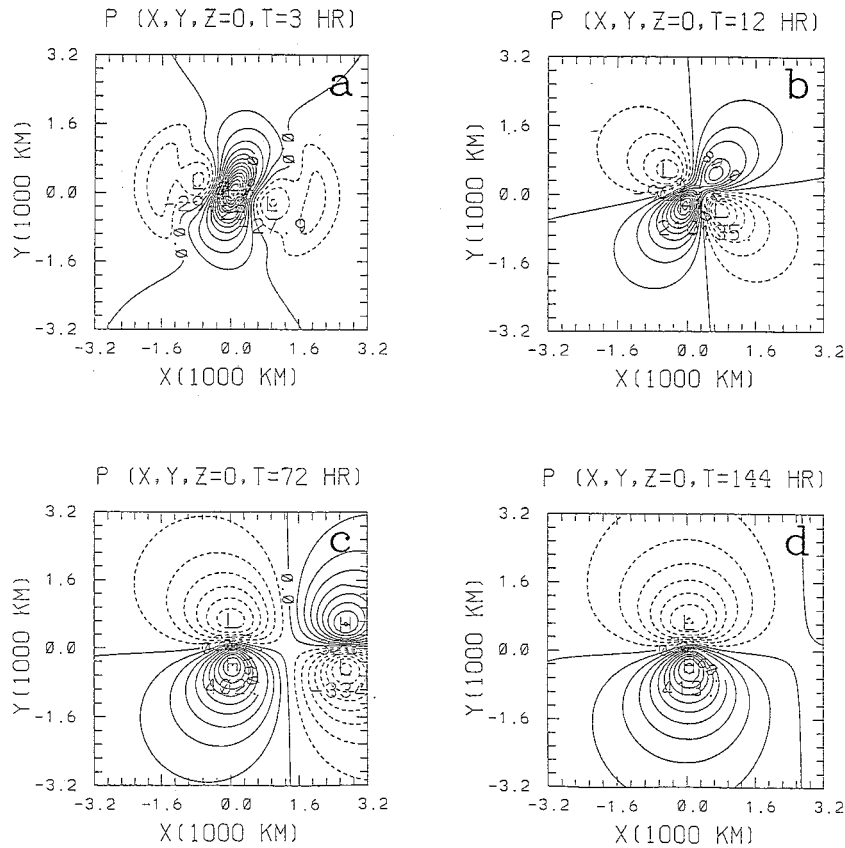
FIG. 10. Same as Fig. 9 except that the perturbation pressure p' at $z = 0$ at (a) $t = 3$ h, (b) $t = 12$ h, (c) $t = 72$ h, and (d) $t = 144$ h is shown. The contour intervals for (a)–(d) are, respectively, 0.09 mb, 0.20 mb, 0.40 mb, and 0.40 mb.

motion and have centers located at approximately $x = \pm 1280$ km, yielding a zonal propagation phase speed of $c_{px} \sim 118.5$ m s^{-1}. Isolated cells of rising motion are located adjacent to those centers of downward motion that are located at $x = \pm 800$ km, yielding $c_{px} \sim 74$ m s^{-1}. Finally, cells of sinking motion straddle the origin at $x = \pm 320$ km. The zonal phase speed associated with these modes is ~ 29.6 m s^{-1}. The vertical wavelength associated with each of these wave modes can be estimated from $c_{px} \sim N/m \sim NL_z/2\pi$, yielding values of 111.7 km, 74.5 km, 46.5 km, and 18.6 km, respectively.

During the subsequent nine hours, although transient IGWs are still radially propagating from the origin, a four-cell pattern in w' begins to form at the forcing center (Fig. 8b) and becomes well defined after the IGWs propagate to far field at later times (Figs. 8c and 8d). The pattern of ascent and descent is simply reversed for $z > 0$ (not shown). This development in w' is related to the transfer of mass by the meridional ageostrophic perturbation winds from the cyclonic to the anticyclonic side of the westerly jet streak in the entrance region (discussed below). This ageostrophic wind pattern is reversed in the exit region of the westerly jet streak.

Figure 9 shows vertical cross sections of u' through

$y = 0$ at $t = 3$, 12, 72, and 144 h. Early during the adjustment ($t = 3$ h), although there is evidence of slight IGW propagation above and below $z = 0$ (Fig. 9a), most of the response is confined to within a distance $\sim O(2d_{jet})$. By $t = 12$ h, a well-defined, isolated couplet of positive and negative zonal wind exists west and east of the forcing center, respectively (Fig. 9b). At later times, the response is dominated by the PV distribution generated by the meridional vorticity gradient of the momentum forcing, which produces an easterly zonal jet streak that is advected downstream at the relative velocity $U - c$ (Fig. 9c), eventually establishing an isolated westerly zonal jet streak of ~ 11.4 m s^{-1} in the vicinity of the forcing region (Fig. 9d).

The pressure perturbation at $z = 0$ and $t = 3$ h (Fig. 10a) is associated with the convergence produced by the alongstream gradient of the perturbation zonal wind couplet on the $z = 0$ plane. At this time, there are two oppositely propagating IGWs whose centers are located roughly at $x \sim \pm 1920$ km. The zonal propagation phase speed associated with these internal modes is approximately $c_{px} \sim 177.8$ m s^{-1}. These modes are relatively weak, being only ~ 0.25 mb in magnitude, or approximately one-fifth the magnitude of the pressure pertur-
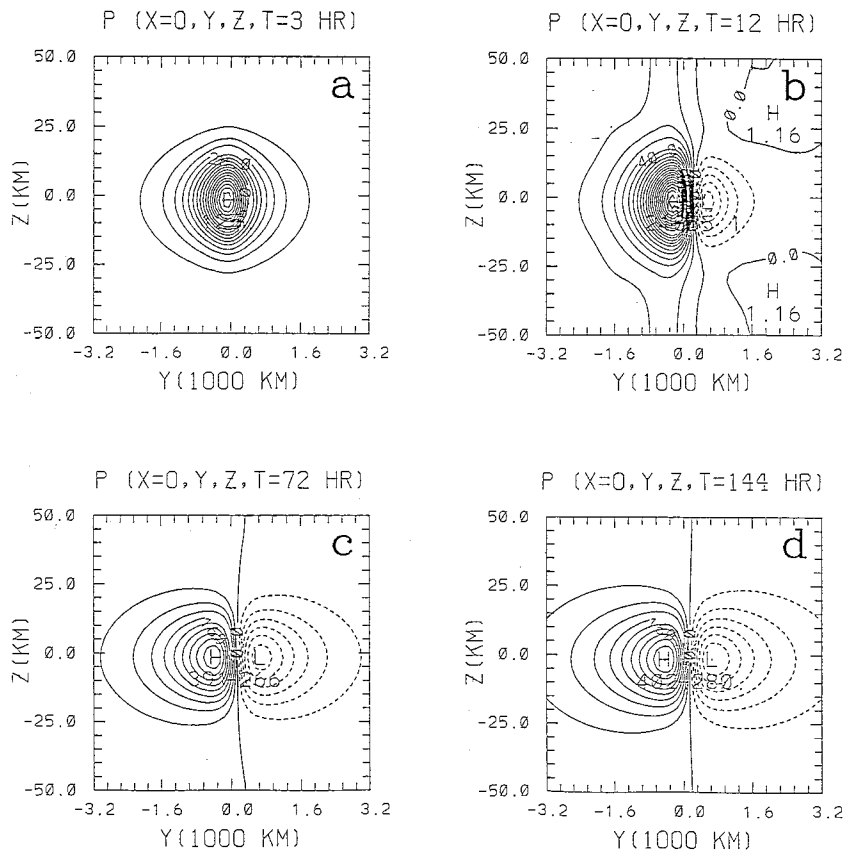
FIG. 11. North–south vertical cross sections of p' associated with the forced geostrophic adjustment at (a) $t = 3$ h, (b) $t = 12$ h, (c) $t = 72$ h, and (d) $t = 144$ h. The contour intervals for panels (a)–(d) are, respectively, 0.07 mb, 0.10 mb, 0.40 mb, and 0.40 mb.

bation colocated with the forcing center. At $t = 12$ h, a well-defined four-cell pattern in p' (Fig. 10b) forms on the $z = 0$ plane. The transfer of mass by the developing ageostrophic winds (shown below) from the cyclonic to the anticyclonic (anticyclonic to the cyclonic) side in the entrance (exit) region of the propagating jet streak effectively lowers/raises the perturbation pressure in the northwest and southeast–southwest and northeast quadrants flanking the jet core (Fig. 8b).

At later times, a perturbation couplet of high (low) pressure north (south) of $y = 0$ exists in the jet exit region, which is advected downstream at the relative velocity $U - c$ (Fig. 10c). This couplet in p' geostrophically supports the easterly zonal jet streak (Fig. 8c) as it is advected downstream. By $t = 144$ h, an isolated couplet of p' exists in the vicinity of the forcing center (Fig. 10d), which geostrophically supports the isolated westerly zonal jet streak (Fig. 9d). The pressure perturbations decrease exponentially with height from the forcing layer in both directions (Fig. 11).

Horizontal cross sections of θ' at $z = -15$ km (Fig. 12) have a structure very similar to the corresponding p' fields (Fig. 10). At $t = 3$ h, an isolated region of warm air of ~ 0.26 K is colocated with the center of

the momentum forcing and is flanked by isolated regions of cold air to its immediate east and west. The warm region is produced adiabatically by the downward vertical motion induced by the convergence of the perturbation zonal winds towards the center of the forcing region (Fig. 8a). At later times (e.g., $t = 12$ h and 72 h), dipoles of warm–cold air located north–south of $y = 0$, which form the externally forced thermodynamic jet streak exit region response, are being advected downstream by the basic-state relative flow, leaving localized regions of cold/warm air north/south of the westerly zonal jet streak by $t = 144$ h, whose centers are colocated with the isolated cells of perturbation low/high perturbation pressure (Fig. 10d).

Figure 13 shows the vertical cross sections of θ' at $x = 0$. Isolated regions of perturbation cold/warm air above/below the $z = 0$ plane at $t = 3$ h (Fig. 13a) are in hydrostatic balance with the perturbation pressure field at $z = 0$ (Figs. 10a and 11a). At later times, such as $t = 12$ and $t = 72$ h (Figs. 13b and 13c), a well-defined couplet of cold (warm) air north (south) of $y = 0$ at all levels below the forcing center is becoming established to hydrostatically balance the perturbation pressure p' (Figs. 10b and 10c), which geostrophically
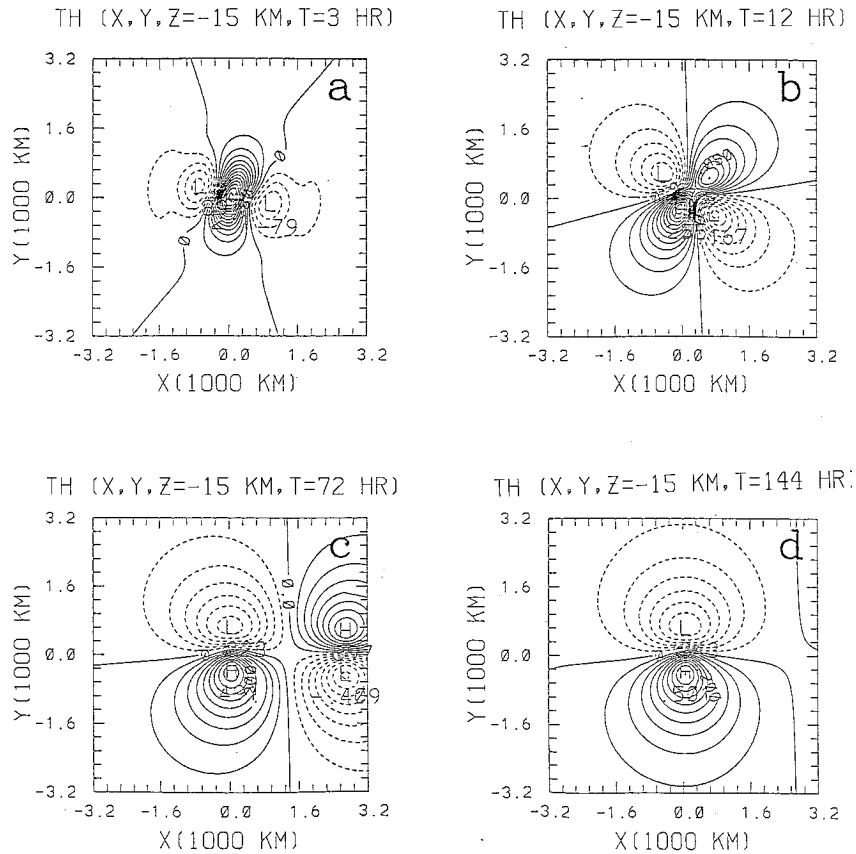
FIG. 12. Same as Fig. 10 except for θ'. The contour intervals for (a, b) and (c, d) are, respectively, 0.02 K and 0.05 K.

supports the externally forced zonal and meridional perturbation winds. This vertical structure in θ' remains essentially unchanged for $t \geq 72$ h (Fig. 13d).

Figure 14 shows $\mathbf{V}'_g$ on the $z = 0$ km plane at $t = 48$ and 72 h (Figs. 14a and 14b), and $\mathbf{V}'_a$ superimposed on the horizontal divergence fields (Figs. 14c and 14d) at the same times. Horizontal cross sections of the vertical motion (Fig. 8), as well as the overall temporal evolution of the forced response (Fig. 14) show that by this time, the transient IGWs that are excited by the prescribed zonal momentum forcing (21) have propagated to the far field. A partitioning of the forced zonal and meridional wind perturbations reveals that both easterly and westerly geostrophic zonal jets are present at these times (Figs. 14a and 14b). The maximum geostrophic wind at $t = 48$ and 72 h is 11.9 and 12.5 m s^{-1}, respectively. The slow increase in the maximum value is due to the steady zonal momentum forcing. The length and width of the westerly geostrophic zonal jet streak at $t = 72$ h are 1760 km and 320 km, respectively, which has the same scales as the westerly zonal jet streak (Fig. 8c). A well-defined cyclonic/anticyclonic circulation of $\sim$ 960 km diameter flanks the westerly/easterly zonal jet core, and is associated with perturbation return flow around the high–low couplet in p'. The easterly geostrophic jet, similar to the

easterly zonal jet (Fig. 8c) is advected downstream at the relative velocity $U - c$ (Fig. 14b).

By $t = 48$ h (Fig. 14c), the ageostrophic flow induced by the acceleration–deceleration dipole of zonal momentum forcing is characterized by a localized cyclonic circulation roughly colocated with the forcing center. The magnitude of this cyclonic circulation at $t = 48$ h is 2.73 m s^{-1}, and therefore is rather weak compared to the corresponding geostrophic component (Fig. 14a). This ageostrophic circulation transports mass from the cyclonic to the anticyclonic side of the westerly zonal jet streak, and in doing so, establishes a four-cell pattern of horizontal divergence that flanks the westerly zonal jet core and produces the four-cell pattern of vertical motion (e.g., Fig. 8c). This ageostrophic flow remains unchanged for all times greater than this (Fig. 14d). The *reversed* nature of these transverse agesotrophic circulations, that is, thermally indirect in the geostrophic jet (Figs. 14a and 14b) entrance region and thermally direct in the exit region, can be explained as follows. The Rossby number characterizing the basic zonal flow is given by $R_{o,U} = (U - c)/2af = 0.1$. Therefore, the forced, linear zonal momentum equation may be approximated as

$$f v'_a = \frac{Du'_g}{Dt} - F_x = \frac{\partial u'_g}{\partial t} + (U - c)\frac{\partial u'_g}{\partial x} - F_x. \quad (27)$$
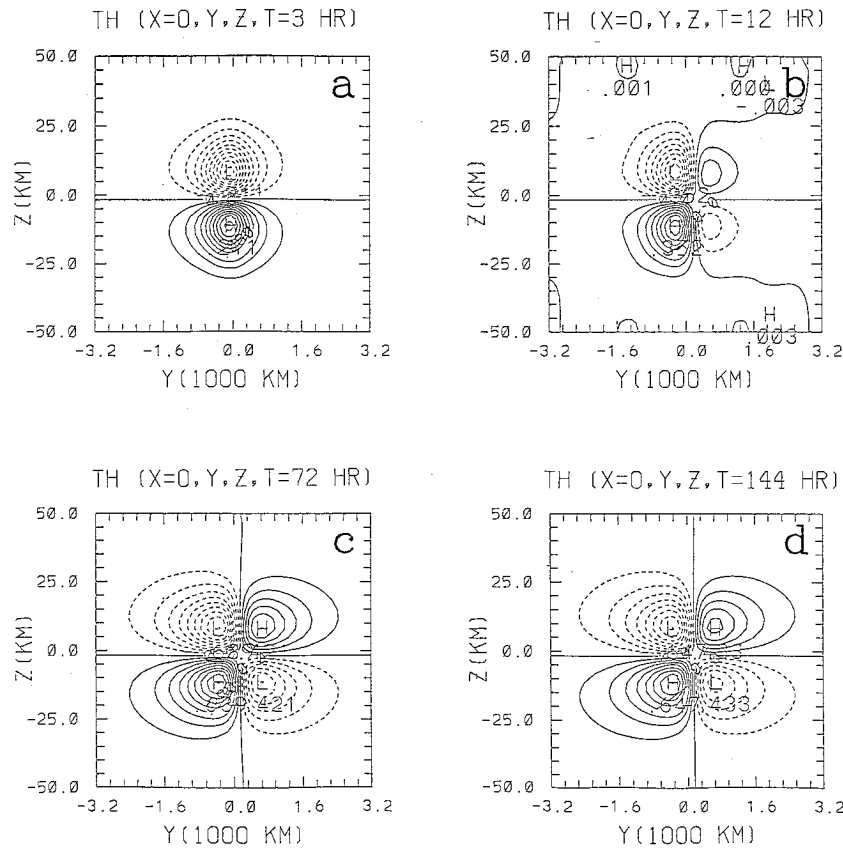
FIG. 13. Same as Fig. 11 except for θ'. The contour intervals for (a)–(d) are, respectively, 0.02 K, 0.04 K, 0.07 K, and 0.08 K.

Using the quasigeostrophic approximation, Uccellini and Johnson (1979) as well as Bluestein (1993) argue that the ageostrophic winds in the entrance and exit regions at the jet core level are normally dominated by nonlinear inertial advection, that is, $u'_g \partial u'_g / \partial x$. The corresponding *linear* process is incorporated through the $(U - c) \partial u'_g / \partial x$ term in (27). From Figs. 14a and 14b, this term is positive/negative in the geostrophic jet entrance/exit region, which produces $v'_a > 0$ ($v'_a < 0$) in the entrance/exit region. However, from (27) it is evident that both $\partial u'_g / \partial t$ and F_x also contribute to the ageostrophic winds. Because $|u'_{g,\max}| = 11.9$ m s^{-1} (12.5) m s^{-1} at $t = 48$ h (72 h), then $\partial u'_g / \partial t > 0$, which, if acting alone, would produce $v'_a > 0$ ($v'_a < 0$) in the entrance (exit) region. However, v'_a is *negatively proportional* to F_x, the external momentum forcing, which is positive (negative) to the west (east) of $\mathbf{r} = (0, 0, 0)$ [see (21)]. The fact that $v'_a < 0$ ($v'_a > 0$) in the entrance (exit) region (Figs. 14c and 14d) implies that the ageostrophic perturbation wind response is dominated by *the geometry of the imposed zonal momentum forcing* rather than by local time tendencies ($\partial u'_g / \partial t$) or linear inertial advection (($U - c) \partial u'_g / \partial x$) of the geostrophic jet.

Figure 15 shows that the total zonal wind perturbation during the early stages before the formation of the PV

distribution associated with the easterly zonal jet is primarily dominated by confluence toward the forcing center, with a gradual increase in amplitude of both the westerly zonal jet (easterly zonal jet) in the entrance (exit) region of the zonal momentum forcing over time. The downstream advection of the easterly zonal jet is clearly evident for $t \geq 36$ h, leaving, within the vicinity of the forcing center, an isolated westerly zonal jet of ~ 12 m s^{-1}.

Figure 16 shows the asymptotic steady-state part of the forced linear response [last term on the right-hand side of (26)]. Recall that it is this steady-state response that will be seen to propagate downstream at the uniform speed c to a nontranslating observer, and therefore will be identified as the mesoscale circulations associated with a mature, quasi-steady, midlatitude jet streak. The horizontal structure of this asymptotic solution on the x–y plane near and below the forcing center can be inferred from the earlier figures (e.g., Figs. 8d and 10d). The linear theory presented here predicts the existence of an isolated region of maximum zonal winds of approximately 11 m s^{-1}, with compensating negative zonal wind perturbations of roughly -2 m s^{-1} located to the north and south of the main jet core (Fig. 16a). The vertical cross section of the meridional wind perturbation 600 km to the west of the zonal jet core in the jet entrance region (Fig. 15b)
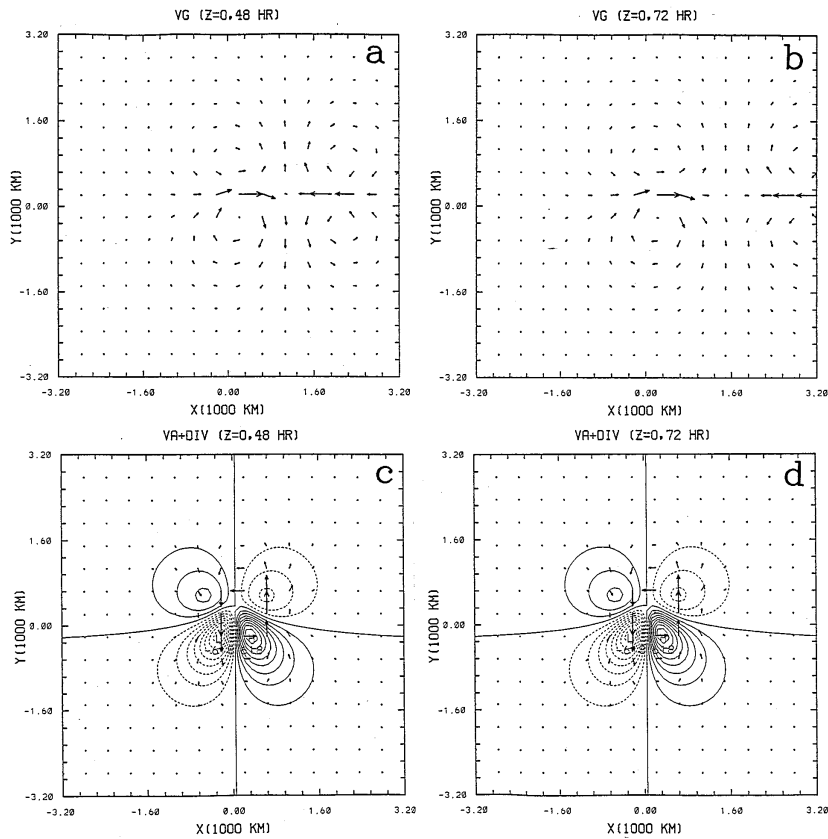
VG (Z=0.48 HR)

VG (Z=0.72 HR)

VA+DIV (Z=0.48 HR)

VA+DIV (Z=0.72 HR)

FIG. 14. Same as Fig. 4 except for the forced response.
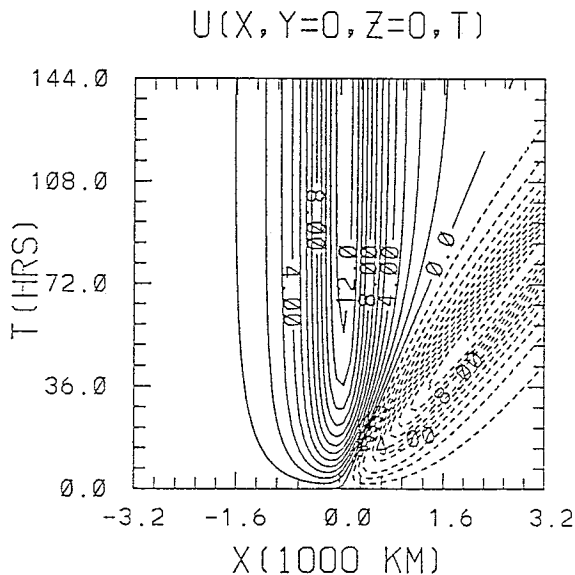
U(X,Y=0,Z=0,T)

FIG. 15. Temporal evolution of the linear response at $z = 0$ in u' as a function of x at $y = 0$ km during the first 144 h of forced adjustment associated with the traveling momentum forcing given by Eq. (21). The contour interval is 1.0 m s^{-1}.

shows that the steady-state confluent flow on the anticyclonic and cyclonic sides of the main jet core is primarily confined to a layer of depth $\sim O(2d_{jet})$. Figures 16c and 16d show the linear steady-state meridional cross sections of p' and θ' fields that support the long-term solution of Figs. 11d and 12d, respectively.

4. Summary and conclusions

A perturbation potential vorticity theory is developed to investigate the three-dimensional, time-dependent, linear geostrophic adjustment of a stably stratified, Boussinesq atmosphere that is disturbed from quiescent equilibrium due to a localized, unbalanced, zonal wind anomaly and geostrophic equilibrium of the uniform zonal flow due to an isolated couplet of acceleration–deceleration forcing. This prescribed zonal momentum forcing propagates downstream at a speed c that is less than the basic-state zonal flow speed U and parameterizes the effects of nonlinear inertial advection.

The transient response shows a relatively wide spectrum of dispersive inertia–gravity waves that can persist for a longer period of time in the zonal direction. The IGWs in the meridional direction in all fields except the vertical velocity are essentially removed in the first 12 h of the response associated with the initial value problem.

U (X=0,Y,Z,T=STEADY)   V (X=600 KM,Y,Z,T=STEADY)

P (X=0,Y,Z,T=STEADY)   TH (X=0,Y,Z,T=STEADY)

FIG. 16. North–south cross sections of the linear steady-state response in a frame of reference moving at the speed of $c = 10$ m s^{-1} produced by the propagating momentum forcing, Eq. (21), in an unbounded Boussinesq atmosphere. This response is defined to be forced quasigeostrophic "jetogenesis." The contour intervals for (a)–(d) are, respectively, 0.70 m s^{-1}, 0.30 m s^{-1}, 0.30 mb, and 0.07 K.

The existence of a uniform zonal flow Doppler shifts the IGWs responsible for removing the initial ageostrophic divergence during the adjustment to geostrophic equilibrium. The steady-state response predicted by linear theory that conserves the initial perturbation PV is a localized, geostrophic zonal jet with meridionally confluent (diffluent) flow in its entrance (exit) region, which is supported by a couplet of perturbation low (high) pressure north (south) of the zonal jet core. At all levels below the level of maximum zonal wind, a couplet of cold (warm) air is colocated with the centers of low (high) pressure on the cyclonic (anticyclonic) side of the isolated zonal jet. This structure in the perturbation potential temperature field is reversed at all levels above the level of maximum zonal wind. The steady-state response characterizes a localized *linear thermal wind* balance among the baroclinic perturbations defining the primary (geostrophic) circulations associated with the geostrophic jet. This balance will not be maintained if nonlinearity is included, and in the absence of prescribed forcing, transverse ageostrophic entrance and exit regions circulations *do not exist.* In order to address this deficiency, the effects of entrance (exit) region acceleration (deceleration) experienced by the

basic-state flow are investigated by considering the response of an unbounded, continuously stratified, uniform zonal flow to a prescribed momentum forcing propagating at the speed $c < U$ through the basic-state current.

As seen by a Galilean observer traveling at the speed $c < U$, the flow response is primarily dominated by the structure of the imposed momentum forcing for $t \leq \tau = 2a/(U - c)$, the advective timescale. During this early stage of adjustment, a localized westerly (easterly) zonal jet exists in the forcing entrance (exit) region due to the initial condition $\partial u'/\partial t = F_x$. The momentum forcing also contributes to the pressure gradient force term in the zonal momentum equation, initially establishing a localized region of perturbation high pressure at the level of maximum zonal winds that is produced by the convergence associated with the alongstream gradient of the perturbation zonal winds. Because the length scales of the forced zonal winds are much less than the characteristic Rossby deformation radius ($L_R \sim 2d_{jet}N/f$), the transient response shows the adjustment of the mass fields to the forced momentum fields. For $t > \tau$, after the transient IGWs have significantly dispersed to the far field, the response is dominated by the circulations associated with

the perturbation PV distribution associated with the meridional gradient of the vorticity generated by the momentum forcing. A portion of this PV distribution produces an isolated easterly zonal jet that is advected downstream at the relative velocity $U - c$, with meridionally diffluent (confluent) perturbation flow in its entrance (exit) region. A dipole of high (low) pressure, which is related hydrostatically to the perturbation potential temperature field, supports this localized easterly zonal jet as it is advected downstream by the zonal flow.

Concurrently, an isolated westerly zonal jet streak with meridionally confluent (diffluent) flow in its entrance (exit) region becomes established in the vicinity of the forcing center. This localized zonal jet streak is supported by a localized region of low/high perturbation pressure north/south of $y = 0$. This pressure couplet is related hydrostatically to the perturbation potential temperature field, and produces primary (geostrophic) circulations similar to that predicted by the linear theory for the initial value problem. The secondary (ageostrophic) circulations transfer mass from the cyclonic to the anticyclonic (anticyclonic to the cyclonic) side of the jet core in the forcing entrance (exit) region, yielding a well-defined four-cell pattern of vertical motion in the quadrants flanking the jet core. These transverse ageostrophic circulations are *reversed* from traditional nonlinear quasigeostrophic jet streak dynamics, because the forced accelerations from the imposed zonal momentum forcing dominate those produced by local time rates of change and linear inertial advection.

Recently, Kaplan et al. (1996a,b), through high-resolution meso-β-scale numerical simulations using a sophisticated mesoscale model initialized with observed data, have identified mesoscale jet streaks or ''jetlets'' that are produced through geostrophic adjustment processes as mesoscale convection perturbs a preexisting meso-α- to synoptic-scale jet streak embedded within the polar jet stream. They define the resulting jetlet as being *unbalanced,* because the secondary entrance and exit region circulations are reversed from those normally associated with observed small Rossby number quasi- or semigeostrophically balanced synoptic-scale jet streaks. Although diabatic forcing is not considered in our study, it is known that momentum transport and its correct parameterization play an important role in mesoscale convective systems. However, the dynamics associated with this transport process are still not well understood. Therefore, the reversed ageostrophic jet streak circulations as predicted by our linear PV theory are not totally unrealistic in the real atmosphere.

APPENDIX

Coefficients, Dispersion Relations, Initial Conditions, and Source Terms for the Initial Value and Forced Geostrophic Adjustment Problems

a. The initial-value problem

The coefficients $R(\mathbf{k})$ for each of the baroclinic perturbations $\phi' = (\mathbf{u}', p',$ or $\theta')$ governed by the linearized wave equation (16) are

$$R(\mathbf{k}) = \begin{cases} \dfrac{ilN^2}{m^2}\hat{q}_i(\mathbf{k}), & \text{if } \phi' = u' \\[2mm] -\dfrac{ikN^2}{m^2}\hat{q}_i(\mathbf{k}), & \text{if } \phi' = v' \\[2mm] 0, & \text{if } \phi' = w' \\[2mm] -\dfrac{\rho_0 N^2 f}{m^2}\hat{q}_i(\mathbf{k}), & \text{if } \phi' = p' \\[2mm] -\dfrac{iN^2\theta_0 f}{gm}\hat{q}_i(\mathbf{k}), & \text{if } \phi' = \theta'. \end{cases} \qquad (A1)$$

The dispersion relationship associated with (16) can be derived:

$$\omega_{\pm} = \Omega \pm f\sqrt{1 + \frac{N^2\kappa^2}{m^2f^2}}, \tag{A2}$$

which indicates that there exists an *infinite* number of length scales or Rossby deformation radii, $L_{R,m} = N/(fm)$, *one for each internal baroclinic mode* of vertical wavenumber m. Defining $m = 2\pi/L_z$, where L_z is the vertical wavelength of the transient inertia-gravity waves, we see that the Rossby deformation radius can be rewritten as $L_{R,m} = NL_z/(2\pi f)$. The phase speed of these internal gravity waves is $c_m = N/m = NL_z/2\pi$, and therefore can be related to the phase speed of short waves excited in a rotating homogeneous atmosphere if one defines an "equivalent depth"

$$H_e = \frac{N^2L_z^2}{4\pi^2g}, \tag{A3}$$

for each baroclinic mode (Gill 1982). Because $c_m = N/m$, (16) implies that the horizontal structure of each internal mode in this system evolves exactly as that predicted by linear shallow-water theory, if the constant undisturbed depth ($H = c_0^2/g$) of that system is replaced by the appropriate equivalent depth H_e for the specific vertical mode $m = 2\pi/L_z$.

The initial conditions for w', $\partial\mathbf{u}_i'/\partial t$, $\partial\theta_i'/\partial t$, and $\partial p_i'/\partial t$ needed to solve the corresponding initial-value problem associated with the impulsive introduction of an unbalanced zonal wind anomaly u_{jet} into a stably stratified atmosphere are taken to be

$$w_i'(\mathbf{r}) = \int_{-\infty}^{z} -\frac{\partial u_{jet}(\mathbf{r})}{\partial x} \, dz, \tag{A4}$$

$$\frac{\partial u_i'}{\partial t}(\mathbf{r}) = -\left(U\frac{\partial}{\partial x} + V\frac{\partial}{\partial y}\right)u_{jet}(\mathbf{r}), \tag{A5}$$

$$\frac{\partial v_i'}{\partial t}(\mathbf{r}) = -fu_{jet}(\mathbf{r}), \tag{A6}$$

$$\frac{\partial w_i'}{\partial t}(\mathbf{r}) = \int_{-\infty}^{z} \left[\frac{\partial}{\partial x}\left(U\frac{\partial}{\partial x} + V\frac{\partial}{\partial y}\right)u_{jet}(\mathbf{r}) + f\frac{\partial u_{jet}(\mathbf{r})}{\partial y}\right] dz, \tag{A7}$$

$$\frac{\partial\theta_i'}{\partial t}(\mathbf{r}) = -\frac{N^2\theta_0}{g}w_i'(\mathbf{r}), \quad \text{and} \tag{A8}$$

$$\frac{\partial p_i'}{\partial t}(\mathbf{r}) = \int_{-\infty}^{z} -\rho_0 N^2 w_i'(\mathbf{r}) \, dz. \tag{A9}$$

The coefficients of Eq. (17) can be determined as

$$A_\phi(\mathbf{k}) = \frac{\hat{u}_{jet}(\mathbf{k})}{2}\begin{cases} \dfrac{(N^2k^2 + m^2f^2)}{(N^2\kappa^2 + m^2f^2)}, & \text{if } \phi' = u' \\[2ex] \dfrac{klN^2}{(N^2\kappa^2 + m^2f^2)} + \dfrac{ifm}{\sqrt{N^2\kappa^2 + f^2m^2}}, & \text{if } \phi' = v' \\[2ex] -\dfrac{1}{m}\left(k + \dfrac{ilfm}{\sqrt{N^2\kappa^2 + f^2m^2}}\right), & \text{if } \phi' = w' \\[2ex] -\rho_0 N^2\left[\dfrac{ilf}{(N^2\kappa^2 + m^2f^2)} + \dfrac{k}{m\sqrt{N^2\kappa^2 + f^2m^2}}\right], & \text{if } \phi' = p' \\[2ex] \dfrac{\theta_0 N^2}{g}\left[\dfrac{lmf}{(N^2\kappa^2 + m^2f^2)} - \dfrac{ik}{\sqrt{N^2\kappa^2 + f^2m^2}}\right], & \text{if } \phi' = \theta' \end{cases} \tag{A10}$$

$$B_\phi(\mathbf{k}) = \left\{ \frac{\left[\left(\sqrt{\frac{N^2\kappa^2}{m^2} + f^2} - \Omega\right)A_\phi(\mathbf{k}) + \lambda\hat{u}_{\text{jet}}(\mathbf{k})\right]}{\left[\sqrt{\frac{N^2\kappa^2}{m^2} + f^2} + \Omega\right]} \right\},$$

(A11)

where

$$\lambda = \begin{cases} \Omega\dfrac{(N^2k^2 + m^2f^2)}{(N^2\kappa^2 + m^2f^2)}, & \text{if } \phi' = u' \\[2ex] \left[-if + \dfrac{klN^2\Omega}{(N^2\kappa^2 + m^2f^2)}\right], & \text{if } \phi' = v' \\[2ex] i\left[\dfrac{(ik\Omega + lf)}{m}\right], & \text{if } \phi' = w' \\[2ex] \rho_0 N^2\left[\dfrac{k}{m^2} - \dfrac{ilf\Omega}{(N^2\kappa^2 + m^2f^2)}\right], & \text{if } \phi' = p' \\[2ex] \dfrac{\theta_0 N^2}{g}\left[\dfrac{ik}{m} + \dfrac{lfm\Omega}{(N^2\kappa^2 + m^2f^2)}\right], & \text{if } \phi' = \theta'. \end{cases}$$

(A12)

b. The forced problem

The inhomogeneous source terms for the linearized potential vorticity and wave equations [Eq. (22)] are

$$G_\xi(q', F_\xi) = \begin{cases} -\dfrac{\partial F_\xi(\mathbf{r}_\xi, t)}{\partial y}, & \text{if } \phi' = q' \\[2ex] -N^2\dfrac{\partial q'(\mathbf{r}_\xi, t)}{\partial y} + \dfrac{\partial^2}{\partial z^2}\left[\left\{\dfrac{\partial}{\partial t} + (U-c)\dfrac{\partial}{\partial\xi} + V\dfrac{\partial}{\partial y}\right\}F_\xi(\mathbf{r}_\xi, t)\right], & \text{if } \phi' = u' \\[2ex] +N^2\dfrac{\partial q'(\mathbf{r}_\xi, t)}{\partial\xi} - f\dfrac{\partial^2 F_\xi(\mathbf{r}_\xi, t)}{\partial z^2}, & \text{if } \phi' = v' \\[2ex] -\dfrac{\partial}{\partial z}\left\{\left[\dfrac{\partial}{\partial t} + (U-c)\dfrac{\partial}{\partial\xi} + V\dfrac{\partial}{\partial y}\right]\dfrac{\partial F_\xi(\mathbf{r}_\xi, t)}{\partial\xi} - f\dfrac{\partial F_\xi(\mathbf{r}_\xi, t)}{\partial y}\right\}, & \text{if } \phi' = w' \\[2ex] \rho_0 N^2\left[fq'(\mathbf{r}_\xi, t) + \dfrac{\partial F_\xi(\mathbf{r}_\xi, t)}{\partial\xi}\right], & \text{if } \phi' = p' \\[2ex] \dfrac{\theta_0 N^2}{g}\dfrac{\partial}{\partial z}\left[fq'(\mathbf{r}_\xi, t) + \dfrac{\partial F_\xi(\mathbf{r}_\xi, t)}{\partial\xi}\right], & \text{if } \phi' = \theta', \end{cases}$$

(A13)

where $\mathbf{r}_\xi = (\xi = x - ct, y, z)$. The coefficients $C(\mathbf{k})$ and $D(\mathbf{k})$ of Eq. (26) are found to be

$$C_\phi(\mathbf{k}) = \begin{Bmatrix} il^2N^2 \\ -iklN^2 \\ 0 \\ -\rho_0 lfN^2 \\ -\dfrac{\theta_0 imlfN^2}{g} \end{Bmatrix} \frac{\hat{F}_\xi(\mathbf{k})}{\Omega(N^2\kappa^2 + m^2f^2)}, \quad \text{if } \phi = \begin{Bmatrix} u' \\ v' \\ w' \\ p' \\ \theta' \end{Bmatrix},$$

(A14)

and

$$D_\phi(\mathbf{k}) = \begin{Bmatrix} i(m^2\Omega^2 - l^2N^2) \\ (iklN^2 - m^2\Omega f) \\ \Omega m(lf - ik\Omega) \\ \rho_0 N^2(lf - ik\Omega) \\ \dfrac{im\theta_0 N^2(ik\Omega - lf)}{g} \end{Bmatrix} \frac{\hat{F}_\xi(\mathbf{k})}{\Omega[N^2\kappa^2 + m^2(f^2 - \Omega^2)]}, \quad \text{if } \phi' = \begin{Bmatrix} u' \\ v' \\ w' \\ p' \\ \theta' \end{Bmatrix}. \tag{A15}$$

The dependent initial conditions (ϕ'_i, $\partial\phi'_i/\partial t$) that determine the remaining unknown coefficients $A_\phi(\mathbf{k})$ and $B_\phi(\mathbf{k})$ are taken to be

$$\hat{u}_i(\mathbf{k}) = \hat{v}_i(\mathbf{k}) = \hat{w}_i(\mathbf{k}) = \hat{p}_i(\mathbf{k}) = \hat{\theta}_i(\mathbf{k}) = 0, \tag{A16}$$

$$\frac{\partial\hat{v}_i}{\partial t}(\mathbf{k}) = \frac{\partial\hat{p}_i}{\partial t}(\mathbf{k}) = \frac{\partial\hat{\theta}_i}{\partial t}(\mathbf{k}) = 0, \tag{A17}$$

$$\frac{\partial\hat{u}_i}{\partial t}(\mathbf{k}) = \hat{F}_\xi(\mathbf{k}), \qquad \frac{\partial\hat{w}_i}{\partial t}(\mathbf{k}) = -\frac{k}{m}\hat{F}_\xi(\mathbf{k}), \tag{A18}$$

which yields the coefficients

$$A_\phi(\mathbf{k}) = -\frac{C_\phi(\mathbf{k})}{2} - \frac{D_\phi(\mathbf{k})}{2}\left(1 + \frac{m\Omega}{\sqrt{N^2\kappa^2 + f^2m^2}}\right) - \lambda\frac{im\hat{F}_\xi(\mathbf{k})}{2\sqrt{N^2\kappa^2 + f^2m^2}}, \tag{A19}$$

$$B_\phi(\mathbf{k}) = \frac{[(\sqrt{N^2\kappa^2 + f^2m^2} - m\Omega)A_\phi(\mathbf{k}) - m\Omega C_\phi(\mathbf{k}) + im\lambda\hat{F}_\xi(\mathbf{k})]}{(\sqrt{N^2\kappa^2 + f^2m^2} + m\Omega)}, \tag{A20}$$

$$A_w(\mathbf{k}) = -\frac{m(lf - ik\Omega)}{2[N^2\kappa^2 + m^2(f^2 - \Omega^2)]}\left(1 + \frac{m\Omega}{\sqrt{N^2\kappa^2 + f^2m^2}}\right)\hat{F}_\xi(\mathbf{k}) + \frac{ik\hat{F}_\xi(\mathbf{k})}{2\sqrt{N^2\kappa^2 + f^2m^2}}, \tag{A21}$$

$$B_w(\mathbf{k}) = \frac{[(\sqrt{N^2\kappa^2 + f^2m^2} - m\Omega)A_w(\mathbf{k}) - ik\hat{F}_\xi(\mathbf{k})]}{(\sqrt{N^2\kappa^2 + f^2m^2} + m\Omega)} \tag{A22}$$

for $\phi' = u'$, v', p', θ', and where $\lambda = 1$ when $\phi' = u'$; otherwise $\lambda = 0$.

REFERENCES

Barwell, B. R., and R. A. Bromley, 1988: The adjustment of numerical weather prediction models to local perturbations. *Quart. J. Roy. Meteor. Soc.,* **114,** 665–689.

Bolin, B., 1953: The adjustment of a non-balanced velocity field toward geostrophic equilibrium in a stratified fluid. *Tellus, 5,* 373–385.

Bluestein, H. B., 1993: *Synoptic-Dynamic Meteorology in Midlatitudes.* Vol. II, *Observations and Theory of Weather Systems.* Oxford University Press, 594 pp.

Blumen, W., 1972: Geostrophic adjustment. *Rev. Geophys. Space Phys.,* **10,** 485–528.

Cahn, A., 1945: An investigation of the free oscillations of a simple current system. *J. Meteor., 2,* 113–119.

Duffy, D. G., 1990: Geostrophic adjustment in a baroclinic atmosphere. *J. Atmos. Sci.,* **47,** 457–473.

Gill, A. E., 1982: *Atmosphere–Ocean Dynamics.* Academic Press, 662 pp.

Holton, J. R., 1992: *An Introduction to Dynamic Meteorology.* Academic Press, 511 pp.

Hoskins, B. J., M. E. McIntyre, and A. W. Robertson, 1985: On the use and significance of isentropic potential vorticity maps. *Quart. J. Roy. Meteor. Soc.,* **111,** 877–946.

Kaplan, M. L., and D. A. Paine, 1977: The observed divergence of the horizontal velocity field and pressure gradient force at the mesoscale: Its implications for the parameterization of three-dimensional momentum transport in synoptic-scale numerical models. *Beitr. Phys. Atmos.,* **50,** 321–330.

——, S. E. Koch, Y.-L. Lin, R. P. Weglarz, and R. A. Rozumalski, 1994a: The numerical simulation of meso-beta scale geostrophic adjustment processes resulting in secondary upper/lower-level jet formation and internal gravity waves during CCOPE. Preprints, *Sixth Conf. on Mesoscale Processes,* Portland, OR, Amer. Meteor. Soc., 382–384.

——, R. A. Rozumalski, R. P. Weglarz, Y.-L. Lin, and S. E. Koch, 1994b: Numerical simulation studies of the role of convectively driven ageostrophic jet streak adjustments in creating a favorable environment for the development of an isolated tornado outbreak. Preprints, *Sixth Conf. on Mesoscale Processes,* Portland, OR, Amer. Meteor. Soc., 144–146.

——, S. E. Koch, Y.-L. Lin, R. P. Weglarz, and R. A. Rozumalski, 1995: The role of a mountains-plains solenoidal circulation in jet streak geostrophic adjustment processes during CCOPE. Preprints, *Seventh Conf. on Mountain Meteorology,* Breckenridge, CO, Amer. Meteor. Soc., 88–95.

——, Y.-L. Lin, D. W. Hamilton, and R. A. Rozumalski, 1996a: The numerical simulation of an unbalanced jetlet and its role in the 1994 Palm Sunday tornado outbreak in Alabama and Georgia. Preprints, *18th Conf. on Severe Local Storms,* San Francisco, CA, Amer. Meteor. Soc., 240–244.

——, ——, R. A. Rozumalski, R. P. Weglarz, and D. W. Hamilton, 1996b: Diabatically-induced geostrophic adjustment processes resulting in unbalanced frontogenesis, shearing instability, and severe weather. Preprints, *Seventh Conf. on Mesoscale Processes,* Reading, England, Amer. Meteor. Soc., 103–108.

Koch, S. E., and P. B. Dorian, 1988: A mesoscale gravity wave event observed during CCOPE. Part III: Wave environment and probable source mechanisms. *Mon. Wea. Rev.,* **116,** 2570–2592.

Lin, Y.-L., 1994a: Airflow over mesoscale heat sources. Part I: Responses in a uniform flow. *Proc. Natl. Sci. Counc.,* **18,** 1–32.

——, 1994b: Airflow over mesoscale heat sources. Part II: Responses in a shear flow. *Proc. Natl. Sci. Counc.,* **18,** 119–150.

Luo, Z., and D. C. Fritts, 1993: Gravity-wave excitation by geostrophic adjustment of the jet stream. Part II: Three-dimensional forcing. *J. Atmos. Sci.,* **50,** 104–115.

Murray, R., and S. M. Daniels, 1953: Transverse flow at entrance and exit to jet streams. *Quart. J. Roy. Meteor. Soc.,* **79,** 236–241.

Namias, J., and P. F. Clapp, 1949: Confluence theory of the high tropospheric jet stream. *J. Meteor.,* **6,** 330–336.

Paegle, J., 1978: The transient mass-flow adjustment of heated atmospheric circulations. *J. Atmos. Sci.,* **35,** 1678–1688.

Pedlosky, J., 1987: *Geophysical Fluid Dynamics.* Springer-Verlag, 710 pp.

Reiter, E. R., 1969: *Jet-Stream Meteorology.* The University of Chicago Press, 515 pp.

Riehl, H., and Coauthors, 1952: *Forecasting in the Middle Latitudes. Meteor. Monogr.,* No. 5, Amer. Meteor. Soc., 80 pp.

Rossby, C. G., 1938: On the mutual adjustment of pressure and velocity distributions in simple current systems, 2. *J. Mar. Res.,* **1,** 239–263.

Schubert, W. H., J. J. Hack, P. L. Silva Dias, and S. R. Fulton, 1980: Geostrophic adjustment in an axisymmetric vortex. *J. Atmos. Sci.,* **37,** 1464–1484.

Smith, R. B., 1979: The influence of mountains on the atmosphere. *Advances in Geophysics,* Vol. 21, Academic Press, 87–230.

——, 1989: Hydrostatic airflow over mountains. *Advances in Geophysics,* Vol. 31, Academic Press, 1–41.

Uccellini, L. W., and D. R. Johnson, 1979: The coupling of upper and lower tropospheric jet streaks and implications for the development of severe convective storms. *Mon. Wea. Rev.,* **107,** 682–703.

——, and S. E. Koch, 1987: The synoptic setting and possible energy sources for mesoscale wave disturbances. *Mon. Wea. Rev.,* **115,** 721–729.

University of Chicago Dept. of Meteorology, 1947: On the general circulation of the atmosphere in middle latitudes. *Bull. Amer. Meteor. Soc.,* **28,** 255–280.

Vallis, G. K., 1992: Mechanisms and parameterizations of geostrophic adjustment and a variational approach to balanced flow. *J. Atmos. Sci.,* **49,** 1144–1160.

van Tuyl, A. H., and J. A. Young, 1982: Numerical simulation of nonlinear jet streak adjustment. *Mon. Wea. Rev.,* **110,** 2038–2054.

Walterscheid, R. L., and D. J. Boucher Jr., 1984: A simple model of the transient response of the thermosphere to impulsive forcing. *J. Atmos. Sci.,* **41,** 1062–1072.

Weglarz, R. P., 1994: Three-dimensional geostrophic adjustment of homogeneous and continuously stratified atmospheres with application to the dynamics of midlatitude jet streaks. Ph.D. dissertation, North Carolina State University at Raleigh, 414 pp.

Williams, R. T., 1965: Nonlinear, non-geostrophic effects in a baroclinic atmosphere. *J. Atmos. Sci.,* **22,** 388–401.

Zack, J. W., and M. L. Kaplan, 1987: Numerical simulations of the subsynoptic features associated with the AVE-SESAME I case. Part I: The preconvective environment. *Mon. Wea. Rev.,* **115,** 2367–2394.

Zhu, X., and J. R. Holton, 1987: Mean fields induced by gravity-wave forcing in the middle atmosphere. *J. Atmos. Sci.,* **44,** 620–630.